MASARYKOVA UNIVERZITA
Přírodovědecká fakulta
Ústav teoretické fyziky a astrofyziky

Diplomová práce

Brno 2026 **Tereza Vaněčková**

MASARYKOVA
UNIVERZITA
PŘÍRODOVĚDECKÁ FAKULTA
ÚSTAV TEORETICKÉ FYZIKY A ASTROFYZIKY

Zkoumání vlastností plazmatu v magnetosférách neutronových hvězd

Diplomová práce

Tereza Vaněčková

Vedoucí práce: Mgr. Jan Benáček, Ph.D. **Brno 2026**

Bibliografický záznam

Autor:	Tereza Vaněčková Přírodovědecká fakulta, Masarykova univerzita Ústav teoretické fyziky a astrofyziky

Název práce:	Zkoumání vlastností plazmatu v magnetosférách neutronových hvězd
Studijní program:	Fyzika
Studijní obor:	Astrofyzika
Vedoucí práce:	Mgr. Jan Benáček, Ph.D.
Akademický rok:	2025/2026
Počet stran:	$14 + 61$
Klíčová slova:	neutronové hvězdy; pulsary,; polární čepičky neutronových hvězd; plazmová produkce párů; particle-in-cell simulace; kvantová elektrodynamika; ACRONYM

Bibliographic Entry

Author:	Tereza Vaněčková Faculty of Science, Masaryk University Department of Theoretical Physics and Astrophysics
Title of Thesis:	Investigating plasma properties in magnetospheres of neutron stars
Degree Programme:	Physics
Field of Study:	Astrophysics
Supervisor:	Mgr. Jan Benáček, Ph.D.
Academic Year:	2025/2026
Number of Pages:	$14 + 61$
Keywords:	neutron stars; pulsars; neutron star polar caps; plasma pair creation; particle-in-cell simulations; quantum electrodynamics; ACRONYM

Abstrakt

Tato diplomová práce se zabývá zkoumáním vlastností plazmatu v magnetosférách neutronových hvězd, především procesem tvorby elektron–positronového plazmatu v oblasti polárních čepiček pulsarů. Jako výzkumnou metodu jsme zvolili particle–in–cell simulace, jmenovitě kód ACRONYM. Před samotným zkoumáním vlastností takového plamatu jsme do kódu implementovali novou metodu pro tvorbu plazmových párů, která bere v potaz i efekty kvantové elektrodynamiky, které se v magnetosférách pulsarů objevují. V této práci popisujeme tuto novou numerickou metodu a výsledky získané s její pomocí.

Abstract

This work focuses on the investigation of plasma properties in the magnetospheres of neutron stars, focusing on the process of electron–positron plasma creation in the pulsar's polar caps. As a research method we are using the particle–in–cell simulations, namely the code called ACRONYM. Before investigating the plasma properties we implemented into the code a new method for plasma pair creation, which takes into account the quantum electrodynamic effects occurring in pulsar's magnetospheres. In this thesis we describe this new numerical method and the results obtained with its usage.

MASARYKOVA UNIVERZITA
PŘÍRODOVĚDECKÁ FAKULTA
KOTLÁŘSKÁ 2, 611 37 BRNO
IČ: 00216224
DIČ: CZ00216224

ZADÁNÍ DIPLOMOVÉ PRÁCE

Akademický rok: 2025/2026

Ústav:	Ústav teoretické fyziky a astrofyziky
Studentka:	Bc. Tereza Vaněčková
Program:	Fyzika
Specializace:	Astrofyzika

Ředitel *ústavu* PřF MU Vám ve smyslu Studijního a zkušebního řádu MU určuje diplomovou práci s názvem:

Název práce:	Zkoumání vlastností plazmatu v magnetosférách neutronových hvězd
Název práce anglicky:	Investigating plasma properties in magnetospheres of neutron stars
Jazyk práce:	angličtina

Oficiální zadání:
After many decades of studies, the mechanisms and formation of electromagnetic emissions and particle acceleration in pulsar magnetospheres remain open question. Though many models study the radiation and acceleration sources from magnetospheric current sheets in the outer magnetosphere beyond the light cylinder, the sources in the inner magnetosphere, especially the polar cap region, are not well understood.

The aim of the thesis is to model plasma pair creation and the particle acceleration in polar cap regions of neutron stars by investigating the plasma properties from particle-in-cell kinetic approach. The polar cap model will be based on current implementation of polar cap kinetic simulations. Specifically, the student will obtain the basic plasma properties and potentially the radiation from particle motion and investigate the formation of plasma bunches/clouds of particles, plasma number and charge densities, bunch velocities, and particle distribution functions. Potentially, also the generated electromagnetic perturbations will be analyzed in terms of the Poynting flux, wave vectors, and intensity. The properties will be produced by simulation data post-processing by using Python in Jupyter Lab environment.

Work plan:
- Study of literature for pulsar magnetospheres and the processes in their polar caps
- Understanding the current polar cap simulations
- Obtaining, compilation, and preliminary run of the ACRONYM code
- Carrying out set of simulations to study various properties of the perturbation
- Processing of the results
- Data interpretation
- Thesis writing

Literature
- Beskin 1993. Physics of pulsar magnetosphere. Book.
- Eilek & Hankins 2016. Radio emission physics of Crab pulsar. J. Plasma Phys.
- Benáček et al. 2024, Poynting flux transport channels formed in polar cap regions of neutron star magnetospheres. arXiv:2405.20866.
- Chernoglazov et al. 2024, Coherence of Multidimensional Pair Production Discharges in Polar Caps of Pulsars. arXiv:2409.15409.

Vedoucí práce:	Mgr. Jan Benáček, Ph.D.
Datum zadání práce:	28. 11. 2024
V Brně dne:	14. 3. 2026

Bc. Tereza Vaněčková, 28. 11. 2024
Mgr. Jan Benáček, Ph.D., 28. 11. 2024
Mgr. Dušan Hemzal, Ph.D., 29. 11. 2024

Poděkování

V první řadě bych ráda poděkovala svému vedoucímu Mgr. Janu Benáčkovi, PhD. za všechen čas, pomoc a podporu, kterou mi za poslední dva roky věnoval. Stejně tak mu patří velké díky za velké množství trpělivosti a jeho důvěru v mé - často pochybné pracovní postupy.
Nejsem moc typ na psaní poděkování, ale tahle diplomová práce by nikdy nevznikla, nebýt podpory lidí v mém okolí, protože celé magisterské studium přineslo do mého života spoustu změn - ať už pozitivních nebo negativních - a bez níže zmíněných bych se v té přehršli nových zkušeností snadno ztratila.
Samozřejmě musím poděkovat své rodině, za milá slova a víkendové obědy. Dále patří obrovské díky mým skvělým spolubydlícím Barče a Nině. Dále také Frantovi s Márou, kteří nám otevřeli dveře, když se jiné zavřely.
Obrovské díky patří i Ondrovi S. mimo jiné i za kontinuální připomínky, že deadliny se blíží. Terce Š. za naše sedánky v knihovně. Kubovi R. za pár nezapomenutelných kocovin.
Nesmím zapomenout ani na kamarády ze skautu, kteří mě pravidelně tahají někam ven vyčistit si hlavu.
A nakonec všem úžasným studentům fyziky, které jsem tady poznala za všechny společné akce a skvělé studijní i nestudijní zážitky.

Prohlášení

Prohlašuji, ze jsem svoji diplomovou práci vypracovala samostatně pod vedením vedoucího práce s využitím informačních zdrojů, které jsou v práci citovány.

Brno 6. května 2026 .....

Tereza Vaněčková

Contents

Introduction

The neutron stars and pulsars are a fascinating field of the astrophysics. The neutron star's pulses are the most precise processes we know. Since the first pulsar was discovered in 1960's we still do not know for sure how exactly the radio emission from the star's jet is created.

Though neutron stars can also give us information about the behavior of plasma in extreme conditions, we are not able to reach such conditions in the Earth's laboratories. Pulsars are objects with very high temperatures and very strong magnetic fields. They also rotate very fast. Therefore, in pulsar's magnetospheric relativistic magnetized plasma corrotates with the star. That leads to many interesting physical phenomena and one of them is electron–positron pair creation. This process we believe that is the main source of pulsar's radio emission. By examining this process we can learn a lot about pulsars but also about plasma itself – and that could be useful in every field of plasma physics.

And how to examine this process? The answer is with simulations, because this is a complex problem, with thousands of charged particles interacting in the electromagnetic field, and it is impossible to find an analytical solution.

In this thesis we work with the particle–in–cell code called ACRONYM, which allows us to simulate, among other processes, the area of the neutron star's polar cap in 2D.

The main aim of our research is to implement a new condition for electron–positron pair creation into this code. This implementation should take into account quantum electrodynamic effects. With this implementation we can then examine various parameters which may impact the plasma behavior.

The objective of this thesis is to describe the influence of these parameters on the simulation and to find out the optimal numerical setup, which could be used in further simulations in this field of study.

Chapter 1

Neutron stars: What are they and how are they formed?

Neutron stars and their magnetospheres are the main objects of this thesis. Their basic characteristic is that they are made of neutrons, but that is definitely not all.

They are super dense, super hot, they have super strong magnetic fields, but also are super small in comparison to classic stars and from the point of the hydrostatic equilibrium equation they are super weird.

Their existence was predicted in the third decade of the last century by Walter Baade and Fritz Zwicky, they were proven theoretically in the 1939 by Robert J. Oppenheimer. That is almost thirty years before Jocelyn Bell discovered the first pulsar, which was later identified as a neutron star.

In this chapter we will look at how they are formed, how they look and how they basically work.

1.1 Neutron star formation

Neutron stars are born by the death of massive stars. They are what remains of the core, when all the nuclear fuel is burned and the gradient of the pressure of the radiation is no longer able to compensate the gravitational force and star collapses.

The lower limit for a star to end like a neutron star is that it has initial mass of eight solar masses (Beskin, Gurevich, and Istomin 1993). These stars are beginning their journey as blue giants, then becoming red supergiants, and their life ends by the explosion of a supernova. The remnant after this supernova is either white dwarf, neutron star, or a black hole.

The key parameter that defines the end of the star is not only the mass of the star itself but also the mass of the carbon-oxygen core. As we see from the Figure 1.1 below, the carbon-oxygen core needs to have mass smaller than two masses of the Sun to become a neutron star and not a black hole.

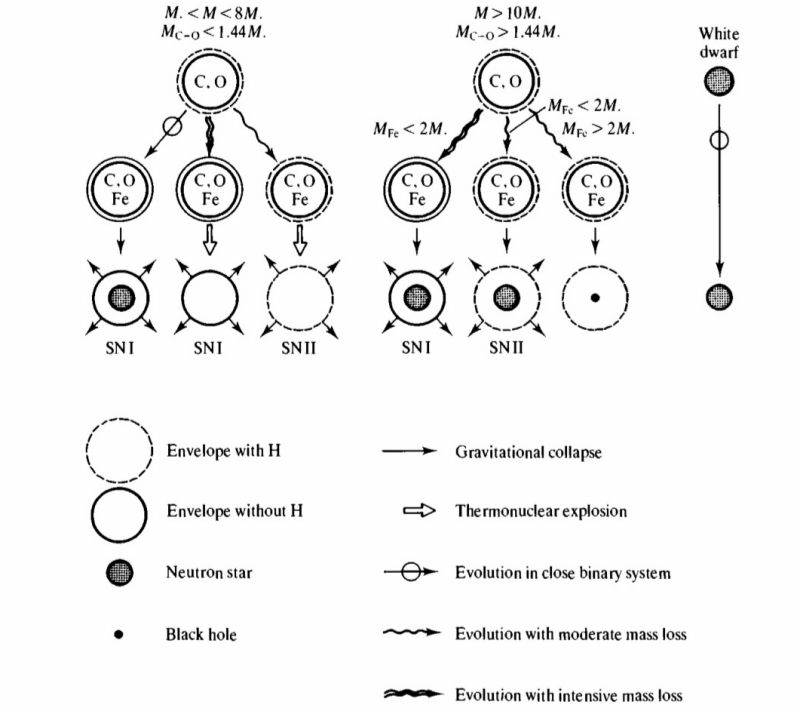

Figure 1.1: Schematic illustration of the neutron star formation (Beskin, Gurevich, and Istomin 1993).

Alternatively, neutron stars can also evolve from the white dwarf in binary systems.

1.2 Basic neutron star properties

As we mentioned before, neutron stars are very small (radius $R = 8 - 15$ km), very dense (density $\rho = 10^{17}$ kg $\cdot$ m^{-3}) and very hot (temperature $T = 10^6$ K) objects (Beskin, Gurevich, and Istomin 1993). When we talk about the mass of these stars, there are models of the star's mass dependence on its radius, based on the solution of the equation of state. From these models we can say that their mass lies between the $(1.4 - 2.7)$ $M_\odot$, where $M_\odot$ is the mass of the Sun.

The upper limit of the star's mass is called the *Tallman-Oppenheimer-Volkoff limit*, and it comes from the equation of the same name

$$\frac{dP(r)}{dr} = -\frac{G[P(r)c^{-2}][m(r) + 4\pi r^3 P(r)c^{-2}]}{r^2[1 - 2Gm(r)r^{-1}c^{-2}]}, \tag{1.1}$$

$$\frac{dm(r)}{dr} = 4\pi r^2 \rho(r), \tag{1.2}$$

$$m(0) = 0. \tag{1.3}$$

Where P stands for the pressure, G for the gravitational constant, c for the speed of light, m for the mass, ρ for the density and r for the distance from the center of the neutron star (ibid.).

One may ask why we are not using the classical equation of the hydrostatic equilibrium? The neutron stars do not behave as "normal" stars because they have absolutely different inner structure.

While in the classical stars, the element acting against the gravitational force is the gradient of the radiation pressure or pressure of matter, in the neutron star cores is happening something else. The atomic nuclei in the core are in such a dense environment that their mutual distance is smaller than the atomic orbital radius. That leads to the application of the *Pauli exclusion principle*, which – as we all know – says that we can not have two electrons of the same system in the same quantum state. And that is, what prevents the collapse of the star.

The other very important characteristics of neutron stars is their strong magnetic field $B \approx 10^{12}$ G. How is it possible?

One possibility is that the magnetic field stays frozen-in during the collapse, therefore it increases with the increasing density in the core, which changes from the 1 g $\cdot$ m^3 to 10^{14} g $\cdot$ m^3, so also the magnetic field intensity changes from 10^2 G to 10^{14} G. Another possible explanation of an unusually strong magnetic field comes from the theory of the thermomagnetic diffusion (ibid.).

1.3 How do neutron stars look like inside?

This is a so far unsolved question. Of course, there are neutrons, which are prevented from decay to proton and neutrinos by a high gradient of the pressure, but otherwise, we still do not know exactly how the body of a neutron star looks.

Whole task of understanding the neutron star's structure is also impeded by the superconductivity, superfluidity and relativistic effects of the matter inside.

We can divide neutron star's parts into the atmosphere, inner crust, outer crust, outer core and inner core.

Atmosphere is made of hydrogen, helium, and carbon.

Outer crust is solid, consisting of atomic nuclei and electrons. It is strongly compressed and contains only a small fraction of the whole mass and is superconductive.

In **inner crust** we can probably find free neutrons and electrons and also nuclei oversaturated by neutrons.

Outer core is just a very dense quantum liquid made from neutrons, protons, and electrons.

And at last, **inner core** is an unknown mixture of proton, neutron, quarks, and maybe even hyperons, but that is something we do not fully understand yet (ibid.).

1.4 Pulsars

The one (and maybe the most important) member of the neutron star's family is the branch of pulsars. These are the neutron stars, whose axis of rotation has a non-zero inclination to the axis of the magnetic field. These objects regularly emit the strong radio beam from the region of their polar caps. The period of these pulses is variable

from millisecond pulses to the periods of a few seconds. And this type of neutron stars is the main focus in this thesis.

The objective of this work is to study the structure of the pulsar pulses, therefore, we will briefly look at how this pulse looks from an observational point of view.

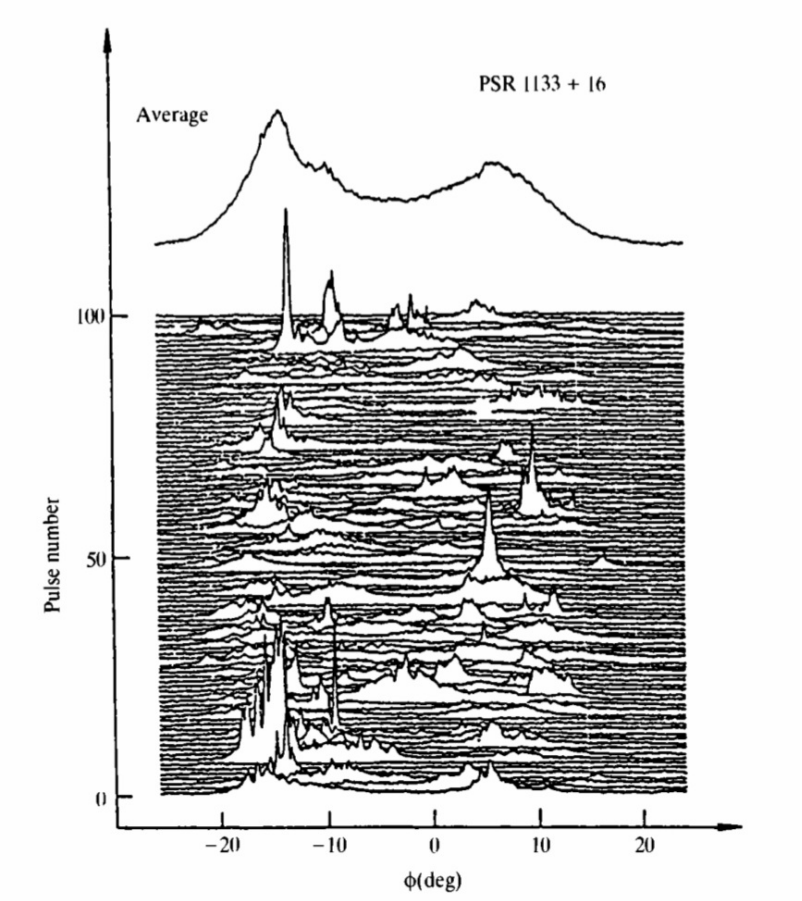

Figure 1.2: Illustration of the various pulses of the neutron star (Beskin, Gurevich, and Istomin 1993).

Figure 1.2 shows the dependency of pulse intensity on the rotational phase of the pulsar. There is illustrated one hundred pulses of one star, and we see that not always they have the same shape and intensity, but their maximum more or less corresponds to one rotational phase. All these pulses can be averaged to a mean pulse shape, as we see on the top part of the figure.

Each single pulse has also its inner structure, which we can see in the Figure 1.3. Here is the time dependency of pulse intensity. Except of the high peak in the middle, there is also a pulse background. This leads us to the idea of energy emitted in a "bunches," that create the interpulses. This will be important further in the discussion of our results.

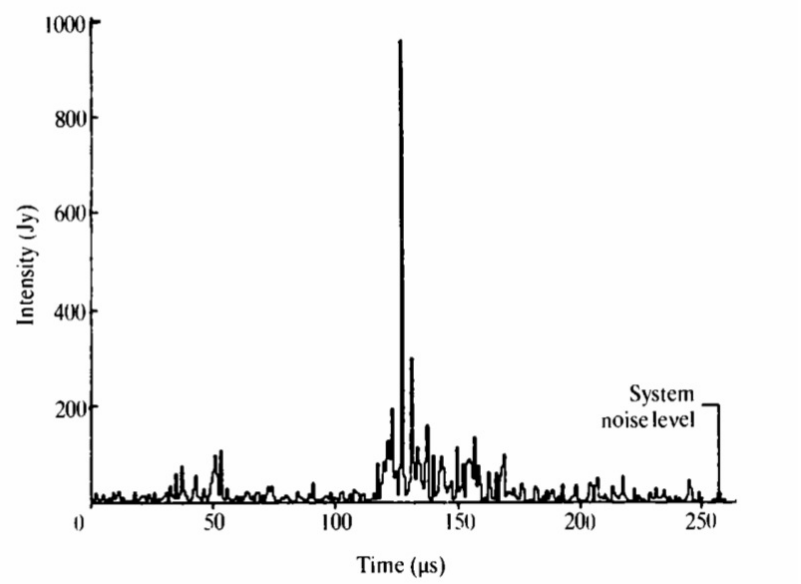

Figure 1.3: Illustration of dependency of pulse intensity on time, with interpulse microstructure (Beskin, Gurevich, and Istomin 1993).

There are many of interesting aspects in the field of pulsars. First, let us at least look at one of the important diagrams connected to the pulsars. It is the $P\dot{P}$ diagram, which is something like the HR diagram for pulsars.

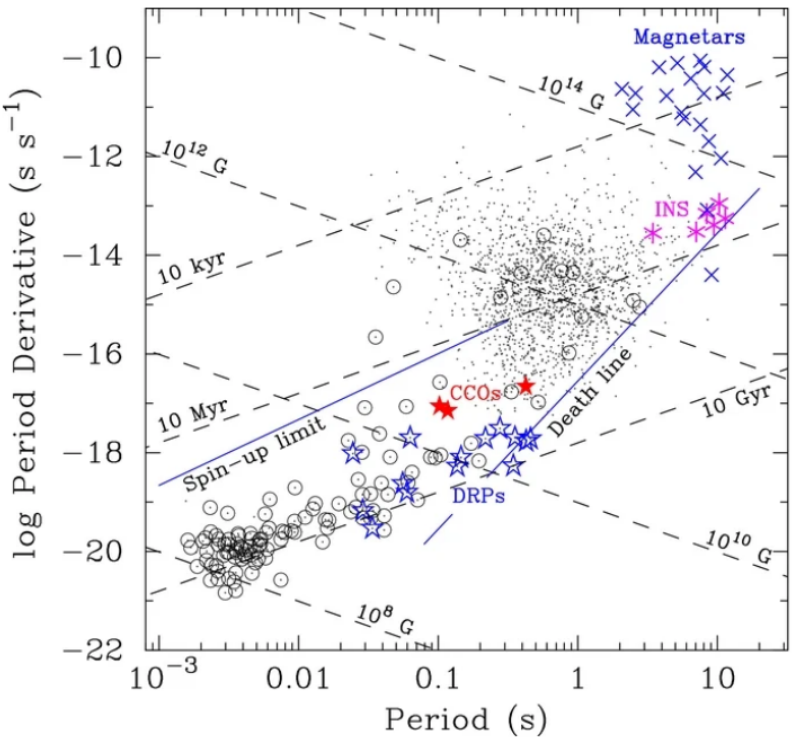

Figure 1.4: $P\dot{P}$ diagram (Gotthelf et al. 2013).

P is here the pulsar period and $\dot{P}$ the period derivative – or in other words it says,

how fast the period P is changing. From this diagram we can read many important properties. For example, how strong is the magnetic field of the pulsar, or how old the pulsar is, or how big energy is radiated from the pulsar.

We can also recognize from it, in which life stadium the pulsar is. Young pulsars have small periods P, which are changing fast. Through time, the pulsar slows down its rotation due to the magnetic dipole radiation and also the stellar wind formation. The period grows, the pulsars move in this diagram forward to the *death line* on the diagram. That is the point where the activity of the magnetospheres decreases, and the pulsar slowly stops emitting radio radiation.

Chapter 2

Plasma: What is it and how does it behave?

Processes that occur in the neutron star polar cap (on which we will be focusing in this thesis) are plasma processes such as the plasma pair creation. Therefore, if we want to understand what is going on, we need to understand the basic concepts of plasma physics.

You have probably heard people saying that plasma is the "fourth state of matter." We define plasma as an ionized gas. But that is not a complete answer.

The classical states of matter are three – gaseous, liquid, and solid. Every state is defined by the thermal energy of the particles of an examined substance. Gaseous particles have the highest thermal energy, solids the lowest. For the phase transition between these states, there must be the latent heat change – addition or subtraction (Bittencourt 2013).

But, that is not what is happening when plasma is created. As we mentioned before, plasma is the ionized gas. The gas, whose temperature and energy were increased so much, that the atoms of the gas were ionized, molecules dissociated and electrons excited.

According to my favourite definition – "plasma is a quasi-neutral gas, consisting of neutrals and positively and negatively charged particles, exhibiting a collective behavior" (Bonaventura 2026).

There are many types of plasma – low temperature, high temperature, atmospheric, low pressure, and others. But all of them need to fulfill the following plasma conditions. All equations in this chapter are defined for the *SI* units.

2.1 Plasma conditions

Before we introduce the conditions for plasma to be a plasma, we need to define two important plasma parameters.
First of them is Debye length

$$\lambda_{\mathrm{D}} = \left(\frac{\varepsilon_0 k_{\mathrm{B}} T}{n_{\mathrm{e}} e^2} \right)^{\frac{1}{2}}, \tag{2.1}$$

where e is the elementary charge, n_e the number of electrons, k_B the Boltzmann constant, T temperature and ε_0 the permittivity of the vacuum. It is a characteristic, which shows to which distance one particle can interact with another.

The other very important quantity is plasma frequency

$$\omega_{\mathrm{pe}} = \left(\frac{n_{\mathrm{e}} e^2}{m_{\mathrm{e}} \varepsilon_0} \right)^{\frac{1}{2}}, \tag{2.2}$$

where again, n_e is the number of electrons, e is the elementary charge, ε_0 the permittivity of the vacuum and m_e is the mass of the electron (Bittencourt 2013).

To understand what the plasma frequency is, imagine following situation. In a quasi-neutral plasma, a small perturbation of electron density is inserted. This perturbation would create a radial electric field. The electrons in the sphere around the perturbation would react to it, and move away from the center of perturbation. However, then the sphere would have a positive charge. The electron would move to the center again and the whole process repeats. The frequency of this process is the plasma frequency.

The plasma frequency is important for counting the plasma skin depth, which is one of the important parameters in plasmas

$$l_{\mathrm{skindepth}} = \frac{c}{\omega_{\mathrm{pe}}}, \tag{2.3}$$

where c is the speed of light.

2.1.1 Macroscopical neutrality

First condition that must be fulfilled is that plasma is macroscopically neutral. We can say it by the equation

$$n_e = \sum_i n_i, \tag{2.4}$$

where the n_e is the number of electrons and n_i is the number of positively charged particles. Naturally, for a substance to be macroscopically neutral it is clear we need to have the same number of negatively and positively charged particles.

In our simulation, this condition is not fully satisfied because we are working on a small area of the neutron star, but for the whole magnetosphere, this condition is fulfilled.

2.1.2 Size of the system

Here comes the time for a Debye length we discussed before. The Debye length is the scale on which the local electric field can be shielded. For the plasma to stay quasi neutral, the size of the whole system must be much greater than Debye length.

$$L \gg \lambda_{\mathrm{D}} \tag{2.5}$$

Here L is the size of the system and λ_{D} is the Debye length.

2.1.3 Number of electrons

Plasma exhibits collective behavior. That means that we need to have more than one particle in a sphere in which they can interact. And the radius of this sphere is defined by a Debye length. Therefore, in Debye's sphere there must be many more particles than one

$$\frac{4}{3}\pi {\lambda_{\mathrm{D}}}^3 n_e \gg 1, \tag{2.6}$$

where n_e is the number of electrons. This condition is also important for a shielding effect that will be discussed later.

2.1.4 Columbian collision frequency

The last condition that needs to be fulfilled for collisionless plasma is that collision frequency between electrons and neutrals must be smaller than plasma frequency

$$\omega_{pl} > \omega_{\mathrm{en}}, \tag{2.7}$$

where ω_{pl} is the plasma frequency and ω_{en} is the collision frequency. In other words, when we define the mean time between two electron-neutral collisions as

$$\tau_{en} = \frac{2\pi}{\omega_{en}}, \tag{2.8}$$

then this time must be longer than the time of the physical changes in the whole plasma system.

It is because the increasing number of electron-neutral collisions has a tendency to reduce plasma oscillations. When we are not dealing with collisionless plasma, this condition does not have to be fulfilled.

In our simulation we can neglect these collisions because this frequency is much lower than the frequency of the changes in polar cap due to plasma pair creation and the plasma frequency.

2.2 Types of plasma

The basic definitions of plasma types are based on the temperature. Though not all parts of plasma have the same temperature, we need to distinguish electron temperature T_e, ion temperature T_i and temperature of gas T_g. When all these temperatures are equal, the plasma is **isothermal**, when they differ, plasma is **non-isothermal**.

Then we make a difference between high and low temperature plasma. For **high temperature** plasma, the mean energy of charged particles is higher than 10^6K, the **low temperature** plasma lower.

In our simulations we deal with relativistic magnetized plasma.

2.3 Plasma in electromagnetic field

Plasma is macroscopically neutral and is still consisting of negatively and positively charged particles. These particles react to external electric and magnetic fields. These fields evolve according to well-known Maxwell's equations.
We introduce the vector of magnetic field intensity $\mathbf{H}$ as

$$\mathbf{H} = \frac{\mathbf{B}}{\mu_0}, \tag{2.9}$$

where $\mathbf{B}$ is a vector of magnetic field induction and μ_0 is the material permeability. And vector of electric induction $\mathbf{D}$ as

$$\mathbf{B} = \mathbf{E}\varepsilon_0, \tag{2.10}$$

where $\mathbf{E}$ is a vector of electric field intensity and ε_0 is the permittivity of the vacuum.

For us will be important, these two from Maxwell's equations (in the material environment)

$$\frac{\partial \mathbf{B}}{\partial t} = -\nabla \times \mathbf{E}, \tag{2.11}$$

$$\frac{\partial \mathbf{D}}{\partial t} = \nabla \times \mathbf{H} - \mathbf{j}, \tag{2.12}$$

where $\mathbf{j}$ is a current density vector (Nishikawa et al. 2021).

First of them is the law of electromagnetic induction, or *Faraday's law*, which says to us that when the external magnetic field changes, the electric current is induced. The second equation is then the *Amper's law*, that claims that the total current depends on changes of the electric induction vector in time and rotation operator applied on the vector of magnetic field intensity.

2.3.1 Plasma motion in electromagnetic field

The basic equation of a motion of charged particles in an electromagnetic field is the Lorentz equation

$$\frac{d\mathbf{p}}{dt} = q(\mathbf{E} + \mathbf{v} \times \mathbf{B}), \tag{2.13}$$

where $\mathbf{p}$ is the particle's momentum, q the charge of the moving particle, $\mathbf{E}$ the intensity of the electric field, $\mathbf{v}$ the velocity vector and $\mathbf{B}$ the vector of magnetic field induction.

We also define $\mathbf{p}$ as

$$\mathbf{p} = \gamma m \mathbf{v}, \tag{2.14}$$

where m is the mass of the particle and γ is its gamma factor, which can be written as

$$\gamma = \frac{1}{\sqrt{1 - \frac{v^2}{c^2}}}, \tag{2.15}$$

where v is the speed of the particle and c the speed of light.

Basically, the magnetic field is the reason for the circular motion around a so-called gyration center. The electric field then moves the particle "to the side". The final trajectory looks like in the Figure 2.1 below and the motion is called *E×B drift*.

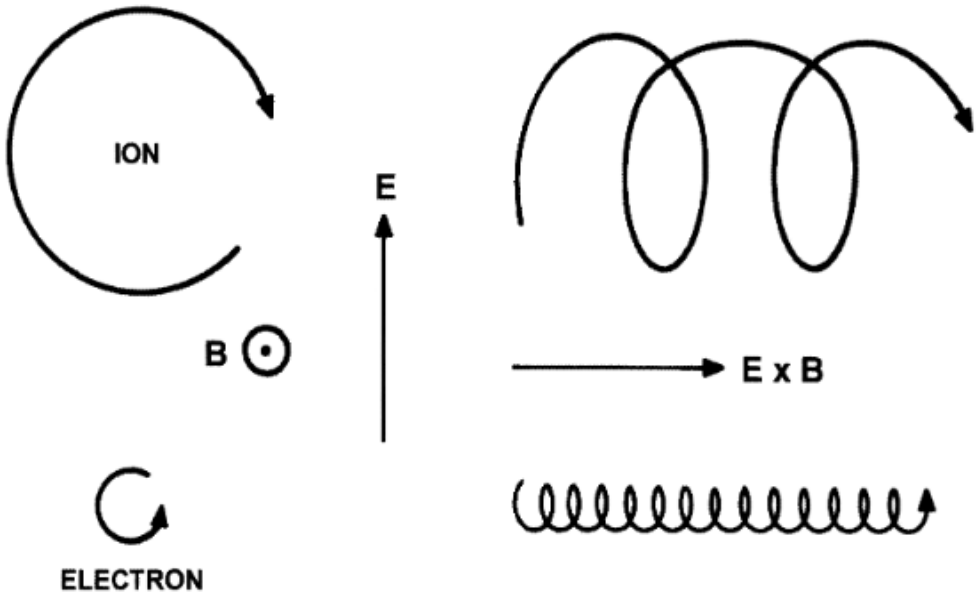

Figure 2.1: Trajectory of a motion of charged particle in electromagnetic field (Bittencourt 2013).

When we assume that the electric field is zero, the particle moves in a circle or a spiral. If we split the velocity into the planar and perpendicular parts and assume that the magnetic field induction vector has only the z-part non-zero, we can rewrite the Equation (2.10) into components as

$$m\frac{dv_x}{dt} = qB_z v_y, \tag{2.16}$$

$$m\frac{dv_y}{dt} = -qB_z v_x, \tag{2.17}$$

$$m\frac{dv_z}{dt} = 0, \tag{2.18}$$

derive them according to time and substitute them into each other, we get

$$\frac{d^2v_x}{dt^2} + \left(\frac{qB_z}{m}\right)^2 v_x = 0, \tag{2.19}$$

$$\frac{d^2v_y}{dt^2} + \left(\frac{qB_z}{m}\right)^2 v_y = 0. \tag{2.20}$$

These equations are the equations of the harmonic oscillator. The frequency of this oscillator is the cyclotron frequency, and it is one of the other important plasma characteristics (Bonaventura 2026)

$$\omega_c = \frac{|q|B_z}{m}. \tag{2.21}$$

Chapter 3

Neutron star magnetospheres: What is happening in there?

The magnetospheres of neutron stars are the main focus of this thesis. Especially the process of plasma pair creation. To understand this process, we need to know how the magnetosphere of this type of object looks.

3.1 Electric field in the pulsar magnetosphere

We need to take into account that inner parts of the neutron star are highly conductive, so we can assume that the magnetic field is frozen-in the neutron star.
For the inner region, the condition must hold

$$\mathbf{E_{in}} + \frac{1}{c}(\mathbf{\Omega} \times \mathbf{r} \times \mathbf{B_{in}}) = 0, \tag{3.1}$$

where $\mathbf{E_{in}}$ is the electric field vector inside the pulsar, $\mathbf{\Omega}$ vector of angular rotation velocity, $\mathbf{r}$ the position vector related to the star centre, c the speed of light and $\mathbf{B_{in}}$ the inner magnetic field (Beskin, Gurevich, and Istomin 1993).

If we remind, that the magnetic field on the surface is of the order $10^{11} - 10^{13}$G, the electric field E on the surface is than reaches the values of:

$$E \sim \frac{\Omega R}{c} B \sim 10^{10} - 10^{12}\mathrm{V}, \tag{3.2}$$

where R is the star radius(ibid.).

Because the magnetosphere is filled by plasma, shielding of parallel components of the electric field occurs.

$$E_{\parallel} \simeq 0. \tag{3.3}$$

The electric potential in the magnetosphere is then non-zero only in the perpendicular direction

$$\phi = \phi(\mathbf{r}_{\perp}). \tag{3.4}$$

This leads to the higher mentioned corotation of plasma in the magnetosphere with the star. To fully understand what exactly is happening (and what also will be important in our simulations) we need to define the *Goldreich-Julian charge density*

$$\rho_c = \frac{\mathrm{div}\mathbf{E_c}}{4\pi} = -\frac{\mathbf{\Omega B}}{2\pi c}. \tag{3.5}$$

The ρ_c is the density of the charge, that is needed for shielding the parallel electric field. The number n_c of particles needed for that is then:

$$n_c = \frac{|\rho_c|}{|e|} = \frac{|\mathbf{\Omega B}|}{2\pi c|e|}. \tag{3.6}$$

And this leads to inducing a corotation current j_c (*Goldreich-Julian current*)

$$j_c = c\rho_c \simeq -\frac{\mathbf{\Omega B}}{2\pi}. \tag{3.7}$$

To imagine how *Goldreich-Julian charge density* looks, we can look at the Figure 3.1 below.

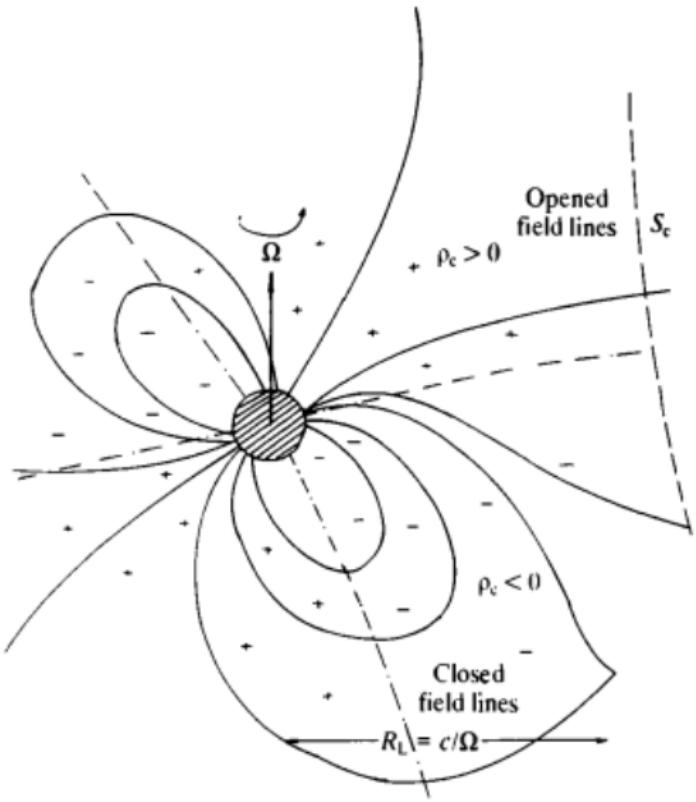

Figure 3.1: Illustration of *Goldreich-Julian charge density* in the magnetosphere of the neutron star (Beskin, Gurevich, and Istomin 1993).

We can see that there are plus and minus signs in different parts of the star's magnetosphere. That is given by the mathematics of vector multiplying and the inclination of the axis of the magnetic field and rotational axis. For an example of a

pulsar for which the inclination angle is zero, the magnetosphere has the shape of the quadrupole.

The *Goldreich-Julian charge density* brings a very important consequence into the creation of plasma pairs in the neutron star's magnetospheres. It is the minimal charge density for a given magnetic field to be frozen-in and corotate with the star. When the density is lower, there is an induced strong electric field that accelerates the charged particles and allows them to react.

3.2 Polar cap of the neutron stars

The magnetic field can be approximated as the dipole field. But because of the corotation, there occurs one interesting phenomenon – closed and opened field lines. And how can a magnetic field line be open?

It is a consequence of the fast pulsar rotation and the corotation of plasma we have discussed before. The farther we are from the star surface, the faster the plasma rotates. And at some point, the plasma is forced to rotate with a velocity close to the speed of light and potentially higher. This is, of course, not possible. Therefore, occurs the distortion of magnetic field and to the "twisting of" the field lines.

The area, where everything "works well" is called the *light cylinder* with the radius

$$R_{LC} = \frac{c}{\Omega}, \tag{3.8}$$

where R_{LC} is the light cylinder radius, Ω the angular velocity and c is the speed of light (Beskin, Gurevich, and Istomin 1993).

The first opened field lines (or the last closed ones) are defining the *polar cap radius*.

$$R_{PC} \simeq R\left(\frac{cR}{\Omega}\right)^{\frac{1}{2}}, \tag{3.9}$$

where R_{PC} is the radius of polar cap (typically around the 200 m for a typicall pulsar) and R is again the radius of the star.

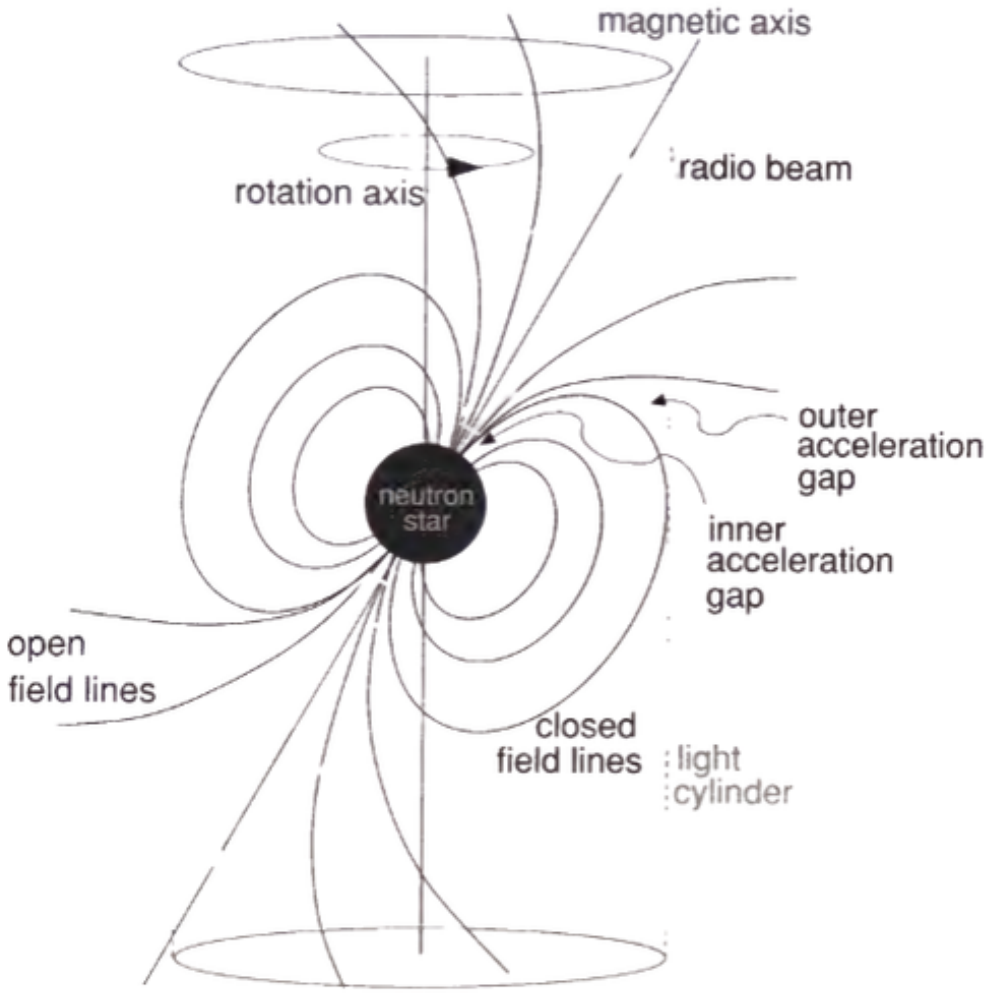

Figure 3.2: Illustration of closed and opened magnetic field lines (Lorimer and Kramer 2005).

When we are close to the star, we can approximate this area of the star as a narrow conical zone, which we are also doing in our simulations.

3.3 Electron–positron plasma creation

One of the processes that may produce the radio emission in pulsar's jets is the electron–positron plasma cascade. There occurs the interaction of photons with magnetic field producing electron–positron pairs.

The maximal electric potential near the surface of the star, is:

$$|\Psi_{max}| \simeq RB_0\left(\frac{\Omega R}{c}\right)^{\frac{3}{2}} \sim 10^{13} - 10^{15}\mathrm{V}, \tag{3.10}$$

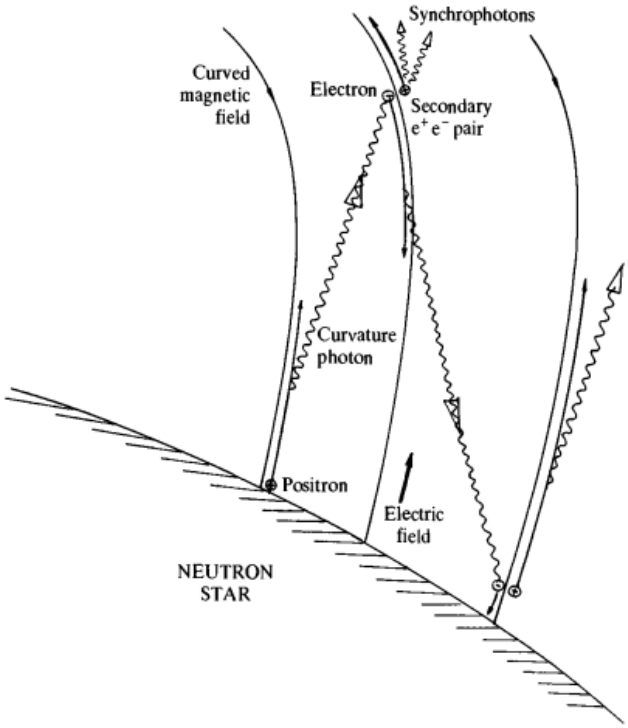

Figure 3.3: Illustration of electron–positron pair creation (Beskin, Gurevich, and Istomin 1993).

where B_0 is the magnetic field strength near the surface (Beskin, Gurevich, and Istomin 1993).

The parallel electric field is then:

$$E_{\parallel} = -\nabla\Psi. \tag{3.11}$$

This electric field accelerates charged particles from the surface. However, because the charged particles are moving in the magnetic field, their trajectory is curved and they radiate curvature radiation. If a photon of this radiation has a high energy, it interacts with the magnetic field and creates an electron–positron pair.

These new particles start to move in the electric field; they can radiate other high energy photons and the cascade continues until the density of charged particles is not high enough to shield the parallel electric field. At this point, the plasma runs out from the magnetosphere, and with decreasing plasma density the parallel electric field can occur again and the whole process starts again.

Chapter 4

Numerical methods: Particle-in-cell simulations and their usage in plasma investigation

Numerical simulations that are discussed in this section help us to solve problems that do not have exact analytical solutions. When we are talking about plasma in a magnetic field of the neutron star, it is exactly this type of problem – because of the collective behavior of plasma. Each particle affects other particles in its Debye's sphere and also interacts with the electromagnetic field.

Numerical simulations allow us to solve Maxwell's equations and the equation of motion for each particle itself. Without the modern approach of numerical simulations, this would not be possible.

4.1 Basics of particle-in-cell simulations

The principle of particle-in-cell (PIC) simulations is, as the name suggests, that we split the space in a finite number of cells and the method works for each cell itself. The time evolution of the process is then also divided into timesteps.
For every cell in every timestep is kept the following cycle (Nishikawa et al. 2021):

- Scatter (Initialization and current deposition)
- Solve (Field solver)
- Gather (Weighting and interpolating)
- Push (Particle pusher)

We now take a closer look at these phases.

Scatter (Initialization and current deposition)

In the first part of the cycle the contributions of the particle to the electromagnetic field are counted – current, charge. And also the particle's properties, especially velocity.

Solve (Field Solver)

Upon the information from the first step, we can now calculate the vector of electric field intensity and magnetic field induction.

Gather (Weighting and interpolating)

Because now we have exact information about electric and magnetic fields, we can calculate the force acting on the particle of our interest.

Push (Particle Pusher)

In the last step, we move the particle into the new position according to its velocity and forces acting on it.

It is good to know that there exists more than one way to go through the whole process. For example, there exists more than one type of the field solver, and also there are more types of particle pushers.

The whole PIC code is of course more complex than what is mentioned above. Not only do the solvers and pushers differ, but there can be different approaches to obtain charge distribution of macroparticle (the concept of macroparticle will be discussed later). There is also a system of sorting particles after every timestep and much more. Every PIC code has its own specifics customized to the problem that it should solve.

4.2 Plasma and PIC simulations

First parameter which is important in the world of PIC simulations is a *macroparticle*. You would probably guess, that it is something as a giant particle – and you would be right. Because we sometimes need to simulate situations with high particle density. If we run the cycle discussed above for each particle itself, there would be high demands on computational power. Therefore, it is easier to create one macroparticle, that represents a chosen number of normal particles and has corresponding weight and charge.

For the discretization of electromagnetic fields in 3D-space is in PIC methods used Yee lattice, coming from the Yee method (a type of finite-difference time-domain method). It is a way to depict electromagnetic fields in one cell of space.

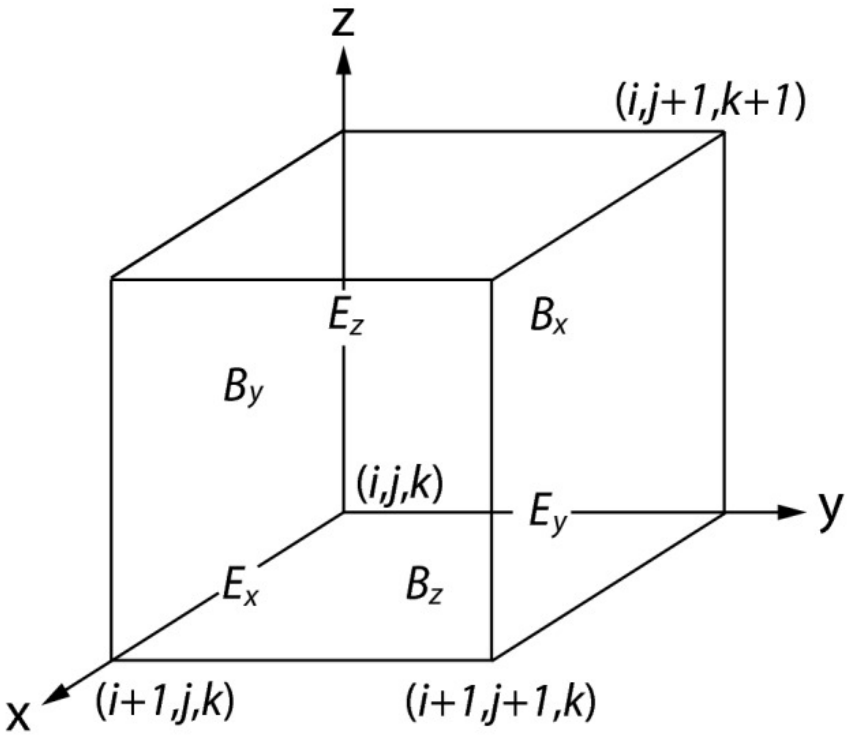

Figure 4.1: Representation of the field components in Yee lattice (Nishikawa et al. 2021).

4.3 ACRONYM code

The code with which we worked on this project is code called ACRONYM; all information about the ACRONYM features in this section was taken from the official website of the code (https://plasma.nerd2nerd.org/, 7.4.2026).

4.3.1 About the code

This code was created by scientists from *prof. Jörg Büchner* group. ACRONYM is the shortcut for the name "Another Code for pushing Relativistic Objects, Now with Yee lattice and Macro particles". Code is managed by a collective of authors and is still evolving.

It is a complex and high-flexible code for simulation in 1D, 2D, and 3D space and it was used for various purposes – from plasma reconnection to collisionless shocks. It is adapted for the work with different species of charged particles. User can choose between different solvers, pushers, shape functions, and current assignments. Also, there is a choice between three types of boundary conditions.

I will not talk about every feature this code offers, only about the ones we have used and why.

ACRONYM pushers

As we mentioned before, pusher is the part of the code which ensures that all particles are moved exactly to the place where they should be after the end of the timestep.

The code offers two pushers – *Boris* and *Vay*. Both of them are defined at half a timestep. We are using the *Vay modification*, which is suitable for particles with relativistic velocities.

ACRONYM solvers

The ACRONYM offers a wide range of solvers. You can use *Electrostatic solver* (not convenient for our electromagnetic plasma), *Radiation free plasma model* (which removes electromagnetic waves) and of course the four types of *Electromagnetic solvers*. The four types are: *Yee grid*, *4th Order solver*, *NSFD solver* and *M24 solver*.

We will use the last mentioned of them. It comes from the *Yee solver* and *4th Order solver*. It has the advantage that against *Yee 2nd order solver* does not have so high wave dispersion in the y-axis and against the *4th Order solver* better suppresses the Cherenkov radiation. It was experimentally shown by supervisor that this field solver is the most numerically precise.

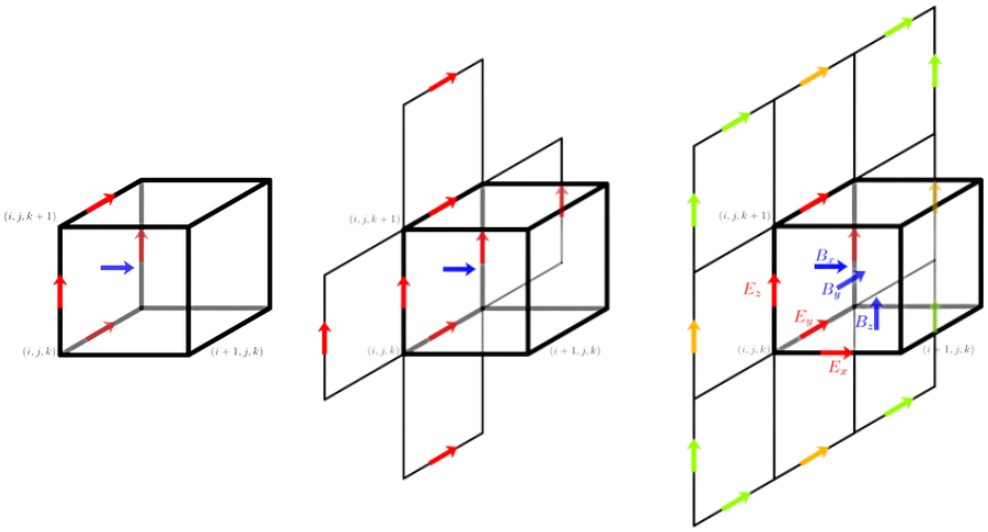

Figure 4.2: Illustration of the various field solvers. From the left: *Yee*, *4th Order*, *M24*. All pictures were also taken from the official ACRONYM website.

ACRONYM shape functions

Shape function describes how the position of the particle is interpolated in and on a grid. This shape also defines the ”shape” of our macroparticle. ACRONYM offers more types of this shape functions. The less complex is the *nearest grid point (NGP)*, which is not numerically exact. Another type is *cloud in cell (CIC)*, where the shape of the function is rectangular. Next type – the one we are using – is the *triangular*

shaped cloud. This is a function that is more complex, has the lower noise and the shape of the function is – of course – triangular.

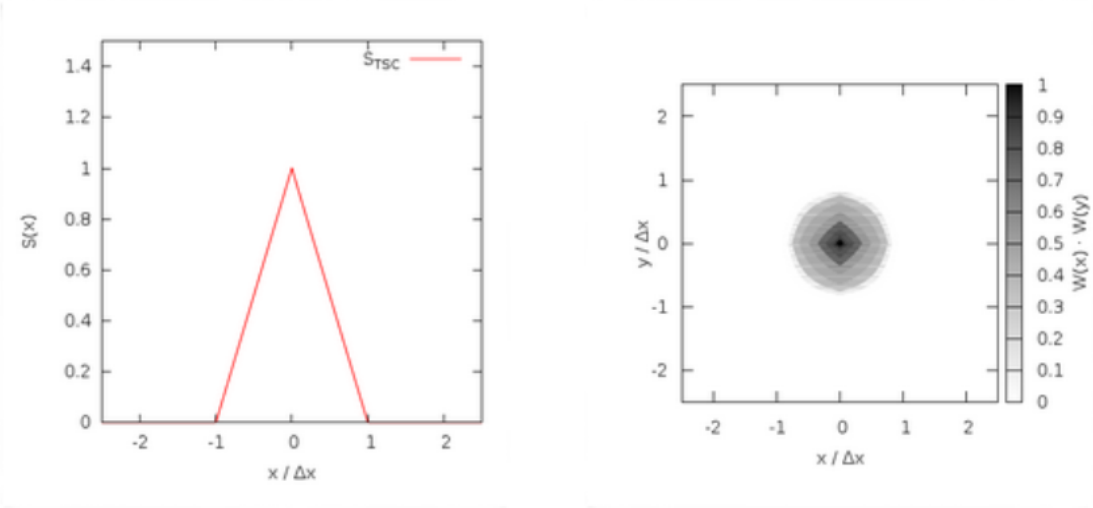

Figure 4.3: Illustration of the *triangular shaped cloud* shape function. All pictures were also taken from the official ACRONYM website.

ACRONYM current deposition

For the right current deposition, we can use two different schemes. One of them is the *Esirkepov scheme*, the other is the *Umeda scheme*. We are using the *Esirkepov scheme*, where the motion of the particle is decomposed into the axis and then weighted and folded together.

With the help of these features, the quantities such as number density or mass are counted.

ACRONYM boundary conditions

When using ACRONYM, one can choose from the three types of boundary conditions. First of them are *periodic boundary conditions*, whose task is basically to take the particles at the border of the simulation and put them on the beginning – in other words – the particles stay all the time in the simulation.

Second type are the *absorbing boundary conditions*, compared to periodic conditions in this type, the particles are at the borders of the simulation absorbed – they ”disappeare”.

Both of these types we have used in this work; in the testing phase, we have used the *periodic conditions*. Later we were using more the *absorbing conditions*.

The last type is the *reflecting boundary conditions*, whose purpose is to reflect the particles at the borders like a mirror.

4.3.2 User environment of ACRONYM

The code is written in C++ and is MPI-parallelized. The language of the code is English and German and is not freely available.

It is needed to have for example a *H5py* library for opening and processing of the simulation data.

For the running of the simulation, the configuration file is needed, in which the user chooses the pusher, solver, etc. The detailed parameters of a concrete simulation are written in the *.cat* file. In this file user can set for example parameters of the neutron star, size of the simulation, and others we will talk about later in the practical part of this work. The example of the *.cat* file can be found in the *Appendix*.

The output of the simulation is in *cgs* units.

4.4 Mathematics behind PIC simulations

In this section we will go through a four basic steps of the PIC simulation and introduce some equations, which were used in our code.

4.4.1 Electric and magnetic field update

For the complex view on the mathematics behind the electromagnetic field updating, we need to first define the electric and magnetic field vector.

$$\mathbf{E} = (e_x, e_y, e_z) \tag{4.1}$$

$$\mathbf{B} = (b_x, b_y, b_z), \tag{4.2}$$

where $e_{x,y,z}$ are the spatial components of the electric field vector, and $b_{x,y,z}$ the spatial components of the magnetic field vector. For this chapter we assume that

$$dx = dy = dz = dt = 1. \tag{4.3}$$

Each component of the electric and magnetic fields is then defined as follows by array indices i, j, k

$$e_x(i,j,k) \to e_x(i+0.5, j, k) \tag{4.4}$$

$$e_y(i,j,k) \to e_y(i, j+0.5, k) \tag{4.5}$$

$$e_z(i,j,k) \to e_z(i, j, k+0.5) \tag{4.6}$$

$$b_x(i,j,k) \to b_x(i, j+0.5, k+0.5) \tag{4.7}$$

$$b_y(i,j,k) \to b_y(i+0.5, j, k+0.5) \tag{4.8}$$

$$b_z(i,j,k) \to b_z(i+0.5, j+0.5, k) \tag{4.9}$$

which means, that the field components are shifted in space. How exactly does the discretization of the electric and magnetic fields look, we see in the Figure 4.1.

And now to the electric field updating itself

$$\frac{\partial \mathbf{E}}{\partial t} = c \begin{vmatrix} \mathbf{i} & \mathbf{j} & \mathbf{k} \\ \frac{\partial}{\partial x} & \frac{\partial}{\partial y} & \frac{\partial}{\partial z} \\ b_x & b_y & b_z \end{vmatrix} = c \left[\left(\frac{\partial b_z}{\partial y} - \frac{\partial b_y}{\partial z} \right) \mathbf{i} + \left(\frac{\partial b_x}{\partial z} - \frac{\partial b_z}{\partial x} \right) \mathbf{j} + \left(\frac{\partial b_y}{\partial x} - \frac{\partial b_x}{\partial y} \right) \mathbf{k} \right], \tag{4.10}$$

where c is the speed of light and b_x, b_y, b_z are the spatial components of the magnetic field induction vector.
The new x component is then

$$e_x^{new}(i,j,k) = e_x^{old}(i,j,k) + c[\{b_z(i,j,k) - b_z(i,j-1,k)\} - \{b_y(i,j,k) - b_y(i,j,k-1)\}]. \tag{4.11}$$

The y and z components can be derived analogically. The magnetic field change in time is counted from an equation similar to Equation (4.10)

$$\frac{\partial \mathbf{B}}{\partial t} = -c \begin{vmatrix} \mathbf{i} & \mathbf{j} & \mathbf{k} \\ \frac{\partial}{\partial x} & \frac{\partial}{\partial y} & \frac{\partial}{\partial z} \\ e_x & e_y & e_z \end{vmatrix} = c \left[\left(\frac{\partial e_y}{\partial z} - \frac{\partial e_z}{\partial y} \right) \mathbf{i} + \left(\frac{\partial e_z}{\partial x} - \frac{\partial e_x}{\partial z} \right) \mathbf{j} + \left(\frac{\partial e_x}{\partial y} - \frac{\partial e_y}{\partial x} \right) \mathbf{k} \right], \tag{4.12}$$

where e_x, e_y, e_z are again the spatial components of the electric field intensity vector (Nishikawa et al. 2021) and the new magnetic field component can be written as

$$b_x^{new}(i,j,k) = b_x^{old}(i,j,k) + c[\{e_y(i,j,k+1) - e_y(i,j,k)\} - \{e_y(i,j+1,k) - e_y(i,j,k)\}]. \tag{4.13}$$

The magnetic field is in the cycle updated two times at half of the timestep.

4.4.2 Particle update – Vay pusher

In this subsection we will briefly go through the mathematics of *Vay pusher*, which we are using in our simulations. All equations from this subsection are taken from the paper Vay 2008. We start with defining the position vector $\mathbf{x}$ of the particle, and its velocity vector $\mathbf{v}$

$$\frac{d\mathbf{x}}{dt} = \mathbf{v}. \tag{4.14}$$

The motion of the particle with charge q and mass m in the electric field $\mathbf{E}$ and magnetic field $\mathbf{B}$ is given by the Lorentz equation

$$\frac{d\gamma\mathbf{v}}{dt} = \frac{q}{m}(\mathbf{E} + \mathbf{v} \times \mathbf{B}), \tag{4.15}$$

where t is time and γ is the relativistic factor

$$\gamma = \frac{1}{\sqrt{1 - \frac{v^2}{c^2}}}, \tag{4.16}$$

where c is the speed of light and v is the size of the velocity vector.

The finite-difference discretization of the position and velocity are

$$\frac{\mathbf{x}^{i+0.5} - \mathbf{x}^{i-0.5}}{\Delta t} = \mathbf{v}^{i}, \tag{4.17}$$

$$\frac{\gamma\mathbf{v}^{i+1} - \gamma\mathbf{v}^{i}}{\Delta t} = \frac{q}{m}(\mathbf{E}^{i+0.5} + \bar{\mathbf{v}}^{i+0.5} \times \mathbf{B}^{i+0.5}), \tag{4.18}$$

where upper indices describe the time evolution of the particle.
The v-barred is

$$\bar{\mathbf{v}}^{i+0.5} = \frac{\gamma^{i}\mathbf{v}^{i} + \gamma^{i+1}\mathbf{v}^{i+1}}{2\bar{\gamma}^{i+0.5}}, \tag{4.19}$$

γ-barred is then written as

$$\bar{\gamma}^{i+0.5} = \sqrt{1 + \left(\gamma^{i}\mathbf{v}^{i} + \frac{q\Delta t}{2m}\mathbf{E}^{i+0.5}\right)} = \sqrt{1 + \left(\gamma^{i+1}\mathbf{v}^{i+1} - \frac{q\Delta t}{2m}\mathbf{E}^{i+0.5}\right)}. \tag{4.20}$$

Therefore, v-barred can be simplified to

$$\bar{\mathbf{v}}^{i+0.5} = \frac{\mathbf{v}^{i} + \mathbf{v}^{i+1}}{2} \tag{4.21}$$

The Equation (4.18) is then rewritten as

$$\frac{\gamma\mathbf{v}^{i+1} - \gamma\mathbf{v}^{i}}{\Delta t} = \frac{q}{m}\left(\mathbf{E}^{i+0.5} + \frac{\mathbf{v}^{i} + \mathbf{v}^{i+1}}{2} \times \mathbf{B}^{i+0.5}\right). \tag{4.22}$$

The heart of Vay's method is in the following equations.

At first, we define vector $\mathbf{u}$ and $\mathbf{u}'$

$$\mathbf{u} = \gamma\mathbf{v}, \tag{4.23}$$

$$\mathbf{u}' = \mathbf{u}^{i} + \frac{q\Delta t}{m}\left(\mathbf{E}^{i+0.5} + \frac{\mathbf{v}^{i}}{2} \times \mathbf{B}^{i+0.5}\right). \tag{4.24}$$

Now, we can rewrite Equation (4.22) as

$$\mathbf{u}^{i+1} = \mathbf{u}' + \frac{q\Delta t}{m}\left(\frac{\mathbf{u}^{i+1}}{2\gamma^{i+1}} \times \mathbf{B}^{i+0.5}\right). \tag{4.25}$$

To solve this equation, we need to know the γ^{i+1}. This value is detailed derived in the higher mentioned article, but we will show only the last step

$$\gamma^{i+1} = \sqrt{\frac{\sigma^2 + \sqrt{\sigma^2 + 4(\tau^2 + u^{*2})}}{2}} \tag{4.26}$$

where σ, τ and u^* are

$$\tau = \left(\frac{q\Delta t}{2m}\right)\mathbf{B}^{i+0.5}, \tag{4.27}$$

$$u^* = \mathbf{u}'\frac{\tau}{c}, \tag{4.28}$$

$$\sigma = \gamma'^2 - \tau^2. \tag{4.29}$$

For the last mentioned parameter we also need the γ'

$$\gamma' = \sqrt{1 + \frac{u'^2}{c^2}}. \tag{4.30}$$

The velocity in the half-timestep can be defined as

$$\mathbf{u}^{i+1} = \frac{1}{1+t^2}[\mathbf{u}' + (\mathbf{u}' \cdot \mathbf{t})\mathbf{t} + \mathbf{u}' \times \mathbf{t}], \tag{4.31}$$

and

$$\mathbf{t} = \frac{\tau}{\gamma^{i+1}}. \tag{4.32}$$

The last step is then to define $\mathbf{u}$ in the half-timestep with help of the velocity vectors in neighboring timesteps

$$\mathbf{u}^{i+0.5} = \mathbf{u}^i + \frac{q\Delta t}{2m}\left(\mathbf{E}^{i+0.5} + \mathbf{v}^i \times \mathbf{B}^{i+0.5}\right) = \mathbf{u}^{i+1} - \frac{q\Delta t}{2m}\left(\mathbf{E}^{i+0.5} + \mathbf{v}^i \times \mathbf{B}^{i+0.5}\right). \tag{4.33}$$

And now, how does the pusher actually work? In the first half of the timestep is counted $\mathbf{u}^{i+0.5}$ from the Equation (4.33).

In the second half of the timestep is counted $\mathbf{u}^{i+1}$ with help of the Equations (4.31), (4.26). For it, we also need to define one last equation

$$\mathbf{u}' = \mathbf{u}^{i+0.5} + \frac{q\Delta t}{2m}\mathbf{E}^{i+0.5}. \tag{4.34}$$

4.4.3 Force interpolation

In this section, we would like to show how the force can be interpolated in PIC simulations. This example would be for first-order interpolation, but we are using the second-order interpolation, which is much more complex.

For the particle in the grid are forces interpolated from the eight nearest entries. In this part of the process, it comes to weighting and weighted volume is defined as (Nishikawa et al. 2021)

$$(1-\delta x)(1-\delta y)(1-\delta z) = c_x c_y c_z. \tag{4.35}$$

Then the force exerted by the electric field in an x-direction is

$$\mathbf{F}_{e_x}^{(x,j,k)} = e_x(i,j,k) + [e_x(i+1,j,k) - e_x(i,j,k)]\delta x. \tag{4.36}$$

The forces in (x,y,k) and (x,y,z) excited by the e_x component of the electric field are

$$\mathbf{F}_{e_x}^{(x,y,k)} = \mathbf{F}_{e_x}^{(x,j,k)} + [\mathbf{F}_{e_x}^{(x,j+1,k)} - \mathbf{F}_{e_x}^{(x,j,k)}]\delta y, \tag{4.37}$$

$$\mathbf{F}_{e_x}^{(x,y,z)} = \mathbf{F}_{e_x}^{(x,y,k)} + [\mathbf{F}_{e_x}^{(x,y,k+1)} - \mathbf{F}_{e_x}^{(x,y,k)}]\delta z. \tag{4.38}$$

Similarly, can be written, the force exerted by the components e_y and e_z. Analogously, then for the forces from the magnetic field.

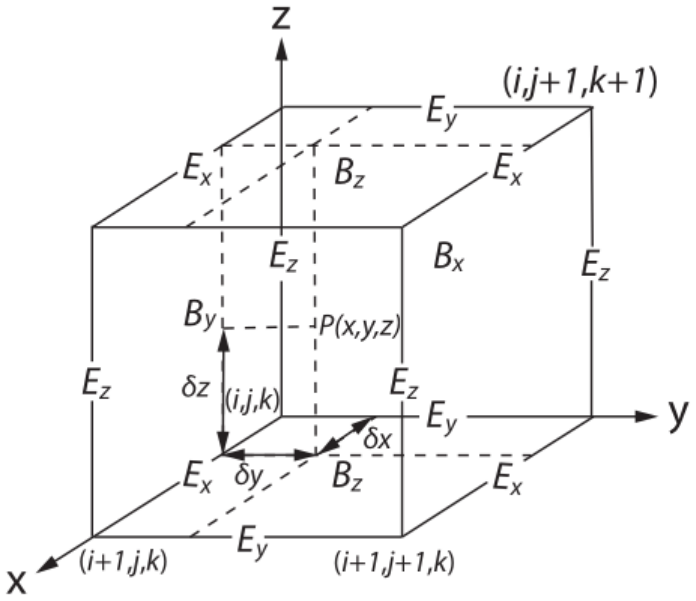

Figure 4.4: Representation of the field components in Yee lattice, where the particle is in position $\mathbf{P} = (x, y, z) = (i, j, k)$ (Nishikawa et al. 2021).

4.4.4 Current deposition

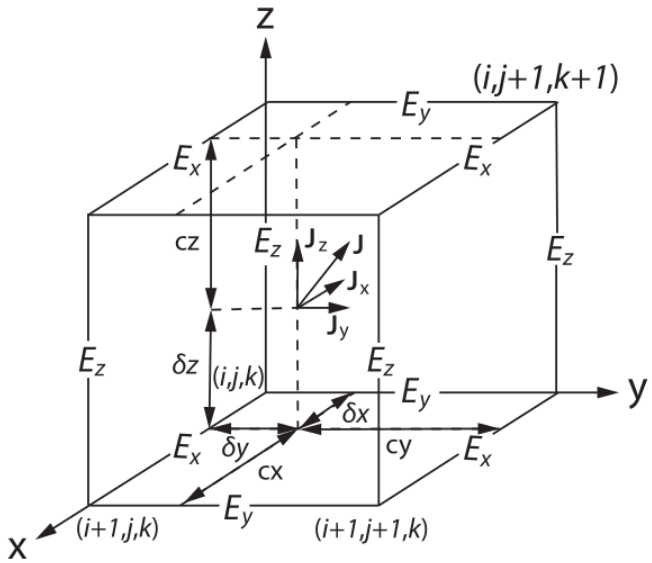

Figure 4.5: Representation of the field components in Yee lattice, where particle is in position $\mathbf{P} = (x, y, z) = (i, j, k)$ (Nishikawa et al. 2021).

In the code the charge conservation condition is satisfied

$$\frac{\partial \rho}{\partial t} = -\nabla \mathbf{J}, \tag{4.39}$$

where ρ is the density and $\mathbf{J}$ is the current density vector.

The current is defined by the charge going through every cell surface carried by particles moving through a cell.

The charge fluxes from x component of the electric field can be written as

$$e_x(i,j,k) = e_x(i,j,k) - J_x \cdot cy \cdot cz \tag{4.40}$$

$$e_x(i,j+1,k) = e_x(i,j+1,k) - J_x \cdot \delta y \cdot cz \tag{4.41}$$

$$e_x(i,j,k+1) = e_x(i,j,k+1) - J_x \cdot cy \cdot \delta z \tag{4.42}$$

$$e_x(i,j+1,k+1) = e_x(i,j+1,k+1) - J_x \cdot \delta y \cdot \delta z \tag{4.43}$$

Analogically are the written charge fluxes in other directions.

Chapter 5

Quantum Electrodynamics: Implementation

In this chapter we will present how exactly our quantum electrodynamics implementation into the ACRONYM works.

In the previous chapter we explained the basics of the PIC simulations. Now we will discuss the whole process of electron–positron pair creation in more detail.

In the first phase of the PIC cycle, we go through every particle in the simulation – electrons, positrons, and photons. We deposit the charge and current of electrons and positrons, and the exact position of all particles.

In the next step, the magnetic and electric fields are solved. Then we can compute the force acting on particles and calculate their velocities.

And here comes the point where we examine if the particles have sufficient energy to create photons. Last step is to count the energy of such created photons and decide if it is enough for electron–positron pair generation.

The next step is then add new particles; if it is needed, remove the particles that created them and go on to the last phase – pushing the particles to the right position.

It is also important to mention that particle can create more than one photon in one timestep, which means that one photon can create more particle pairs.

5.1 Creation condition without QED effects

The basic condition in the 2D version of ACRONYM code for a photon creation was relatively straightforward.

In a *.cat* could the user set a parameter called `gamma_threshold` to a fixed value. This value was then compared to the gamma factor of each single particle. If a particle's gamma factor was higher than this threshold, a new photon that can potentially create a pair, was added to the simulation.

The whole condition can be expressed by an equation

$$\gamma_{particle} > \gamma_{threshold}, \tag{5.1}$$

$$\gamma_{particle} = \frac{1}{\sqrt{1 - \frac{v^2}{c^2}}}, \tag{5.2}$$

where $\gamma_{threshold}$ is the fixed value set by user and v is the value of particle's velocity vector.

5.2 Creation condition with more specific QED effects

The condition we are testing in this thesis is more complicated. We will take it step by step.

At first, we will look closer at the curvature photons production.

Photon creation

The first part of electron–positron plasma creation is curvature radiation. The charged particle moving in the magnetic field changes its trajectory and radiates curvature photons. The critical frequency of these photons is given by

$$\nu_{critical} = \frac{3\gamma^3 c}{4\pi R^2_{curvature}}, \tag{5.3}$$

where γ is the gamma factor of the particle, c the speed of light and $R_{curvature}$ is the radius of the curvature of the star's magnetic field.

Moreover, the photons produced by this process are not monochromatic, but their spectrum is given by the non-analytical integral of Bessel function and the maximum of this function is exactly the $\nu_{critical}$. The numerical expression of this integral is in code written as

$$D_{Bessel} = 2.15x^{\frac{1}{3}} \cdot (1+3.06x)^{\frac{1}{6}} + (1+0.884x^{\frac{2}{3}}) + \frac{0.471x^{\frac{4}{3}}}{(1+1.6x^{\frac{2}{3}} - 0.974x^{\frac{4}{3}})} \cdot e^{-x}, \tag{5.4}$$

where x is defined as the ratio of the photon frequency ν_{photon} and critical frequency

$$x = \frac{\nu_{photon}}{\nu_{critical}}. \tag{5.5}$$

After solving these equations we know the frequency of the created photon and we can estimate its energy

$$E_{photon} = h\nu_{photon}, \tag{5.6}$$

where h is the Planck's constant.

The power of this radiation depends on particle's velocity and curvature radius by equation

$$P_{curvature} = \frac{2e^2u^4}{3c^3R^2_{curvature}}, \tag{5.7}$$

where e is the elementary charge, u the speed of the curved particle (v multiplied by gamma factor γ). And the $R_{curvature}$ is again the radius of the curvature of the magnetic field.

From the power of the radiation we can now easily count the number n of produced photons, which should be created in time interval of duration dt

$$n = \frac{P_{curvature} dt}{E_{photon}}. \tag{5.8}$$

This value n then says if there are some photons to generate or not, by this rule

$$n \geq \gamma_{photon\_emission\_threshold} \rightarrow \text{add photon}, \tag{5.9}$$

$$n < \gamma_{photon\_emission\_threshold} \rightarrow \text{add no photon}. \tag{5.10}$$

The $\gamma_{photon\_emission\_threshold}$ is an arbitrary parameter. Therefore, it gives us the opportunity to create "smaller" or "larger" macroparticles of the size of the fraction of classical macroparticle.

The last parameter we define in this section is the mean free path l, which we are using for deleting the photons with longer l than the spatial scale of our simulation – because such photons do nothing important in the simulation process, only take the computing capacity.

$$l = \frac{8 m_e c^2 R_{curvature}}{3 B E_{photon}} \tag{5.11}$$

The m_e there stands for the mass of the electron and B the magnetic field intensity, which we can set in the *.cat* file.

Particle-pair creation

When we have photons in the simulation, these photons can start to interact with the magnetic field. This interaction depends on the angle between photons trajectory and magnetic field lines and, of course, on the intensity of the magnetic field.

All of this is tied up together by the attenuation parameter α

$$\alpha = \frac{\frac{1}{2}\alpha_0 B_\perp T}{\lambda_e B_{critical}}, \tag{5.12}$$

where $B_\perp$ is the component of the magnetic field perpendicular to the photon's trajectory

$$B_\perp = |\mathbf{n}_{photon} \times \mathbf{B}|. \tag{5.13}$$

The critical size of the magnetic field is

$$B_{critical} = 4.414 \times 10^{13}\text{G}, \tag{5.14}$$

the standard grid parameter α_0

$$\alpha_0 = \frac{1}{137}, \tag{5.15}$$

and the parameters T and λ_e are (Erber 1966)

$$T = 0.46 e^{-\frac{4}{3\chi}}, \tag{5.16}$$

$$\lambda_e = 2.43 \times 10^{-10}\text{cm}. \tag{5.17}$$

For the evaluation of the parameter T we also need to know the value of parameter χ

$$\chi = \frac{1}{2}\frac{E_{photon}}{m_e c^2}\frac{B_\perp}{B_{critical}}. \tag{5.18}$$

This is a very important value, which is smaller than one in our case because the energy ratio is around 10^6 and the magnetic field ratio 10^{-7}.

Another important aspect we need to remind is that the photon, of course, needs to have at least energy equal to the rest energy of the electron–positron pair; otherwise, the photon does not have enough energy for pair creation.

$$E_{photon} > 2m_e c^2 \tag{5.19}$$

When we know the value of attenuation parameter we can define the conversion rate m which tells us how many pairs will be created

$$m = \alpha c dt, \tag{5.20}$$

where cdt is standing there for the length of photon path.

Finally we compare the conversion rate m to a randomly generated number r in range from zero to one in every timestep. The pairs are then created by the rule

$$m \geq r \rightarrow \text{add pair}, \tag{5.21}$$

$$m < r \rightarrow \text{add no pair}. \tag{5.22}$$

Chapter 6

Results: What we have achieved and what is it good for?

In this chapter, we show the most important results of the thesis. The aim of the work was to implement the QED pair creation condition into the 2D version of the code. The main task of mine was then to test and debug the code, carry out simulations, and analyze results.

That entails running tens of different simulations. After the debugging of the code, one looks for the "sweet spot" of all the adjustable parameters, for which was needed also much more attempts. Therefore, we present here only the most important findings of our work.

For evaluation of simulation behavior we used knowledge from the supervisor's article about Poynting flux transport channels in the polar cap region. We also used some of the numerical parameters given in the article as our starting point (Benáček, Timokhin, et al. 2024).

6.1 Preliminary results and numerical problems

We would like to briefly show some of the problems we needed to solve before we started to focus on softer details of the simulations.

For example, looking at the Figure 6.1, you see there are four cross sections through the polar cap. On the x-axis is the width of the polar cap in the simulation grid cell and on the y-axis the height of the simulation above the surface of the star ($x[\Delta] = y[\Delta] = 333.544\text{cm}$).

On the single images we can see – electron density, positron density, charge density and Poynting flux. There can be seen a cross through the whole simulation in the third image. That is a problem caused by the bug in the sorting part of the simulation cycle.

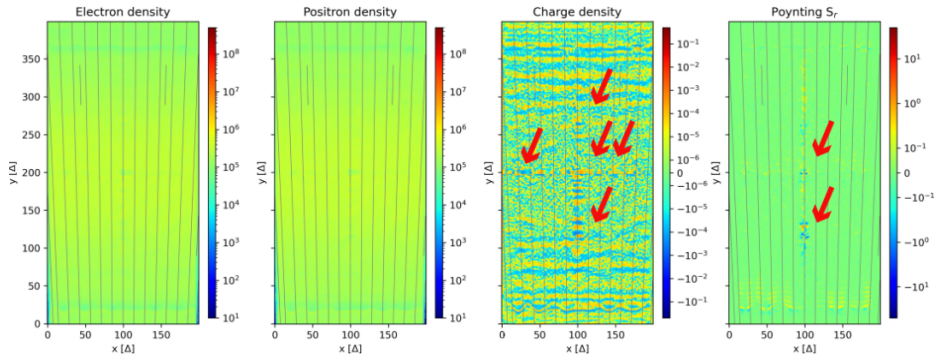

Figure 6.1: Example of a problem with sorting particles. Electron, positron and charge density and Poynting flux are in arbitrary units.

On the next Figure 6.2 we will look closer on the grey lines in the background of the image – they represent a magnetic field lines. They should be almost parallel, but they are twisting in upper corners.

This mistake was eliminated by balancing of some parameters in *.cat* file and by changing of boundary conditions, causing the incorrect wave absorption around the simulation box and eventually causing artificial magnetic field lines twisting.

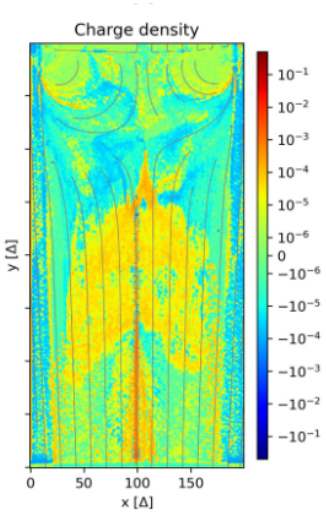

Figure 6.2: Example of the distortion of the field lines in the simulation. Charge density is in arbitrary units.

In the Figure 6.3 we can see one of the smaller simulations, and what we see here is that the simulation is oversaturated with the charged particles. That is not a problem from the physical side of view, but from the view of computing resources.

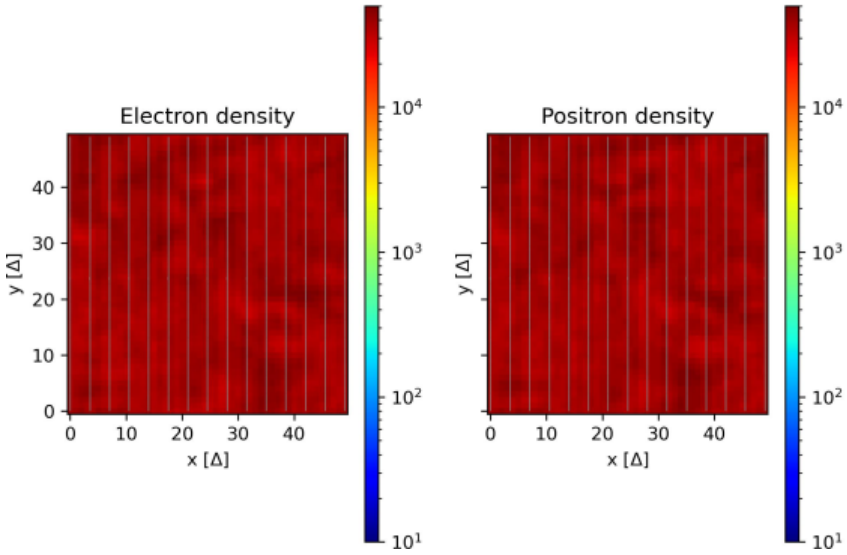

Figure 6.3: Example of simulation oversaturated with the particles. Electron and positron density are in arbitrary units.

Such simulations had high demands on computational time and on the data storage capacities, therefore we applied the method, which declares the maximal number of particles in a cell (by changing the parameter `max_ppc`) to eliminate these problems and have an opportunity to run bigger and longer simulations.

The last of the initial problems we would like to show is in the Figure 6.4. There are sections on the edges where the electron and positron densities are higher than in the middle. That was also something caused by the wrong choice of boundary conditions along x-axis.

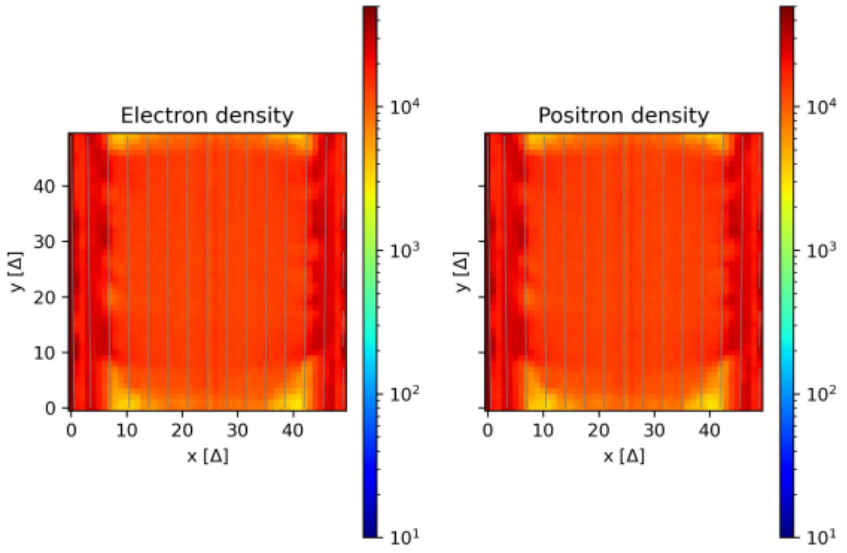

Figure 6.4: Example of wrong choice of boundary conditions. Electron and positron density are in arbitrary units.

6.2 Results of final simulations

After the debugging of the code and balancing all parameters, we come to the one reference simulation (whose *.cat* file you can find in the *Appendix*) that we would like to show in detail.

The size of this simulation is 200×400 grids (667×1334 meters), it is computed in the plan-parallel configuration of the magnetic field lines, with absorbing boundary conditions in the y-axis and the periodic boundary conditions in the x-axis.

Now I would like to introduce four numerical parameters we found out that can have the largest impact on the final results. First of them is `max_ppc`, which restricts the number of particles in a single cell. It helps with the computational time and for the reference simulation, it is equal to one hundred particles per cell.

Second is the `radiation_reaction_photon_emission_threshold`, which tells us, simply said, how "big" can be one photon macroparticle, when the photon is created. We have here some number of single particles in one macroparticle, but in the PIC cycle, there can be a situation that there is created some number of single photons, but their count is not enough to create one photon macroparticle. With the help of this parameter we can add into simulation, for example, ten times smaller macroparticle. For this simulation it is set to one, which corresponds to the size of one classical macroparticle.

The third parameter is the `radiation_reaction_curvature_radius` which declares the curvature of the magnetic field, for this simulation it is 10^9 cm, which corresponds to a classical values for pulsars. And finally, the pair of the parameters `radiation_reaction_nu_min` and `radiation_reaction_nu_max` which defines the frequency range for selecting the random photon frequency from the integral from the approximated Bessel function in the units of $\nu_{critical}$ as discussed in the *Chapter* 5.

For our reference simulation, these parameters are in Table 6.1. In Table 6.2, the other important characteristics of simulation are stated. We are not changing them, and they are the same for all simulations discussed in this work. We are choosing values of radius, mass, period and magnetic field that would correspond to a real neutron star's parameters.

The size of the grid and size of the timestep are scaled such as the potential photon travels in one timestep distance lower than the size of the grid. That is important for a numerical scheme to be stable.

The important adjustable parameters from *.cat* file	
max_ppc	100
`radiation_reaction_curvature_radius`	10^9 cm
`radiation_reaction_photon_emission_threshold`	1
`radiation_reaction_nu_min`	$1 \cdot \nu_{critical}$
`radiation_reaction_nu_max`	$1 \cdot \nu_{critical}$

Table 6.1: List of parameters whose dependencies we are investigating.

The important parameters from *.cat* file	
Width of the simulation x	200 grids
Height of the simulation y	400 grids
Size of one grid	333.544 cm
Timestep Δt	5.56 ns
Boundary conditions in x-axis	periodic
Boundary conditions in y-axis	absorbing
Total simulation time	10 000 timesteps
Output	10 timesteps
R_{star}	10^6 cm
m_{star}	10^{31} kg
T_{star}	0.25 s
Plasma frequency ω_{pl}	4×10^6 s^{-1}
Magnetic field B	10^{12} G
`magnetospheric_current_scale`	5×10^{-7}
`polar_cap_angle`	2.5°
`photon_maximal_distance`	13 421.76 m
`radiation_reaction_gamma_min`	10^7

Table 6.2: Important simulation characteristics, same for all investigated confugurations.

Parameter `photon_maximal_distance` is set to the value, corresponding to a size of simulation domain. Photons with longer maximal distance would not start to create particles in the simulation, therefore, it is not necessary to include them. The `radiation_reaction_gamma_min` declares that for the Lorentz factor γ, smaller than this value we can neglect the energy losses by curvature radiation, which accelerates the computational process. And the parameter `magnetospheric_current_scale` scales the magnetospheric current downward. Reason for this parameter is to ensure that our simulation is able to describe current density with an appropriate number of particles, including preservation of the right Debye length.

Parameter `polar_cap_angle` is set to the value for which we can approximate the magnetic field lines as parallel.

Now we can look at the time dependence of such simulation at the Figures 6.5–6.8. We can see there a dependence of eight parameters - current density parallel, electric field parallel, electric field perpendicular, Poyntig flux, electron density, positron density, charge density and photon density. There a cross section of the polar cap. In the center of x-axis is the magnetic field axis and on the y-axis is the height above the star's surface. The lines on the bottom of all simulations are the representation of star's surface. All quantities are scaled as following

$$J_{\parallel\_scaled} = \frac{J_\parallel}{|\rho_{charge}|}, \tag{6.1}$$

$$E_{\parallel\_scaled} = \frac{E_\parallel}{|E|}, \tag{6.2}$$

$$E_{\perp\_scaled} = \frac{E_{\perp}}{\overline{|E|}}, \tag{6.3}$$

$$S_{r\_scaled} = \frac{S_r}{\overline{|E||B_{ext}|}}, \tag{6.4}$$

$$N_{e\_scaled} = \frac{N_e}{\overline{|N_{particle}|}}, \tag{6.5}$$

$$N_{p\_scaled} = \frac{N_p}{\overline{|N_{particle}|}}, \tag{6.6}$$

$$\rho_{charge\_scaled} = \frac{\rho_{charge}}{\overline{|\rho_{charge}|}}, \tag{6.7}$$

$$N_{photon\_scaled} = \frac{N_{photon}}{\overline{|N_{particle}|}}, \tag{6.8}$$

where on the left-hand side are the scaled parameters, $\overline{|\rho_{charge}|}$ is the mean charge density in the cross section of the simulation, the $\overline{|N_{particle}|}$ is the mean particle density, $\overline{|E|}$ the size of the electric field vector, $\overline{|B_{ext}|}$ the size of the magnetic field vector, $E_{\parallel}$ and $E_{\perp}$ are the components of the electric field vector, $J_{\parallel}$ the parallel component of the charge density vector and S_r is the Poynting flux. All mean values are counted as an arithmetic mean through the whole space domain in a given timestep.

At the Figure 6.5 we can see the higher discussed plasma parameters in the timestep 100 of the simulation. Electrons are starting to move from the surface of the star, positrons are moving towards the star's surface, and no photons are present yet.

In the Figure 6.6 we can see the first created photon cascade, corresponding to lowering number density of electrons and positrons in the middle of height above the surface.

In the timestep 4300 (Figure 6.7) we can see the growing number of photons and their movement from the simulation and also the creation of new electron and positron pairs. What is also interesting here is the evolution of Poynting flux and growing intensity of electric fields. The "bunches" in the Poynting subplot are the evidence that the simulation evolves in a right way (Benáček, Muñoz, and Büchner 2021). On the last Figure 6.8 we can see the process of the evolution of something like a jet in the middle of the simulation area.

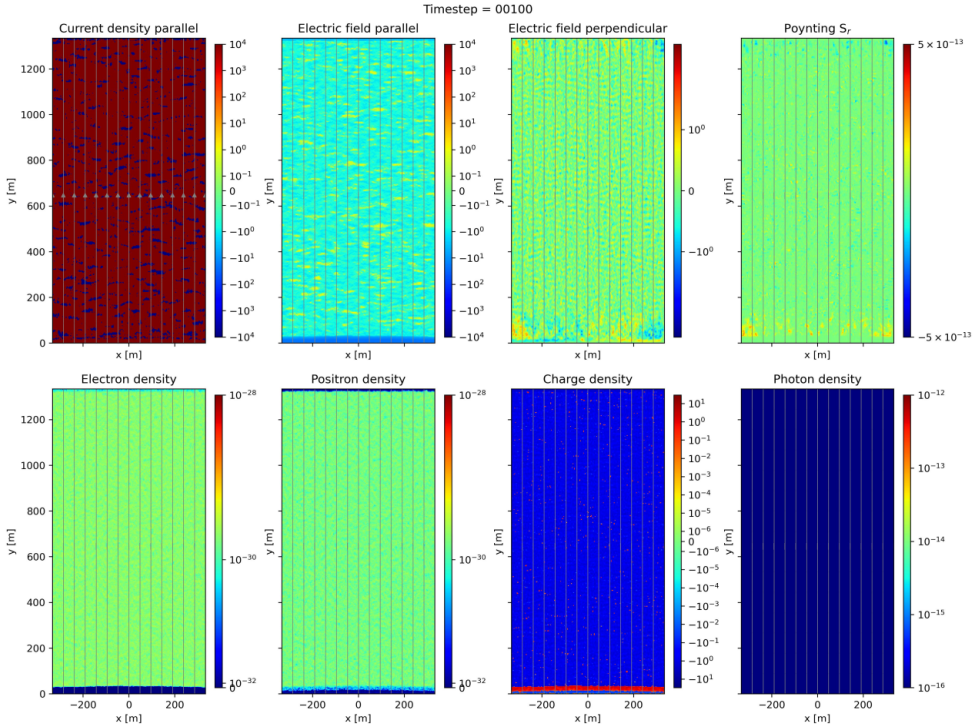

Figure 6.5: Reference simulation in a timestep 100.

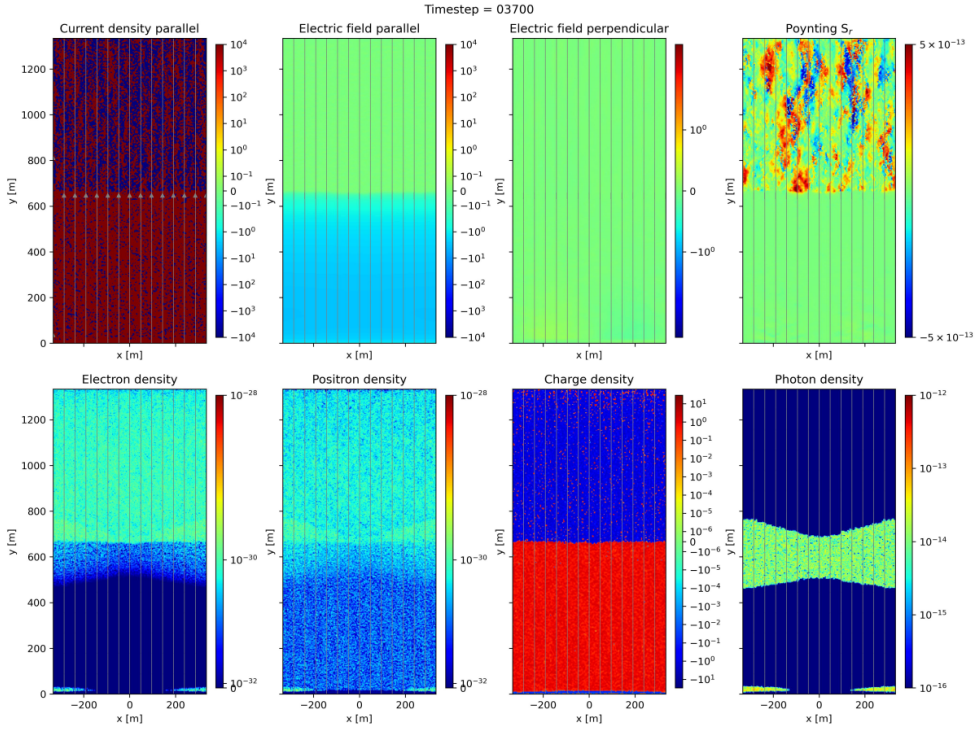

Figure 6.6: Reference simulation in a timestep 3700.

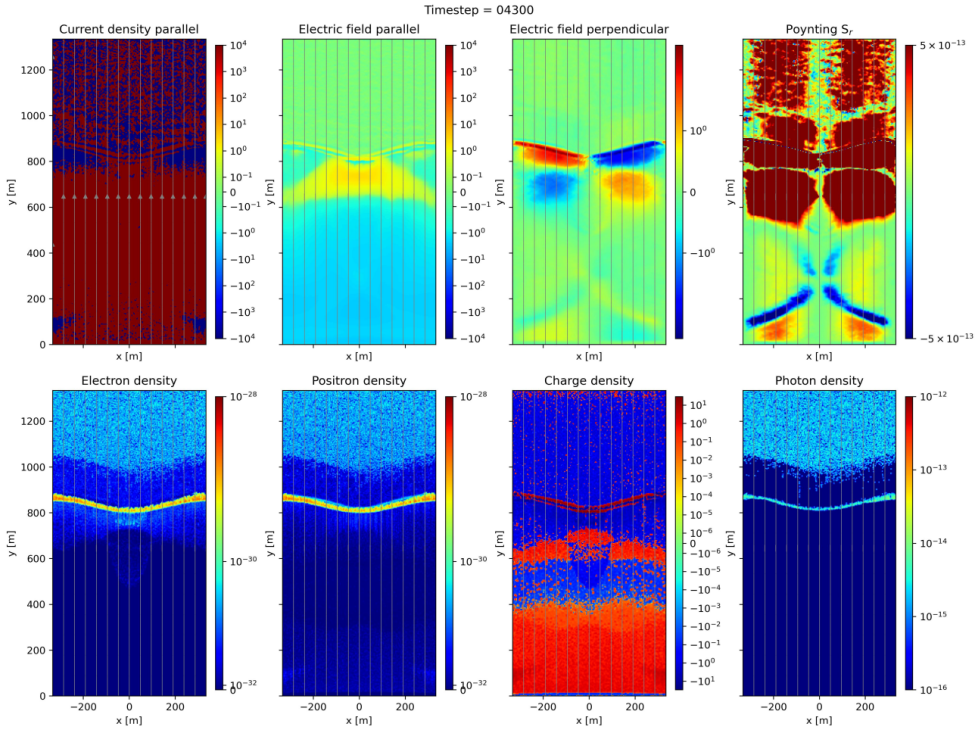

Figure 6.7: Reference simulation in a timestep 4300.

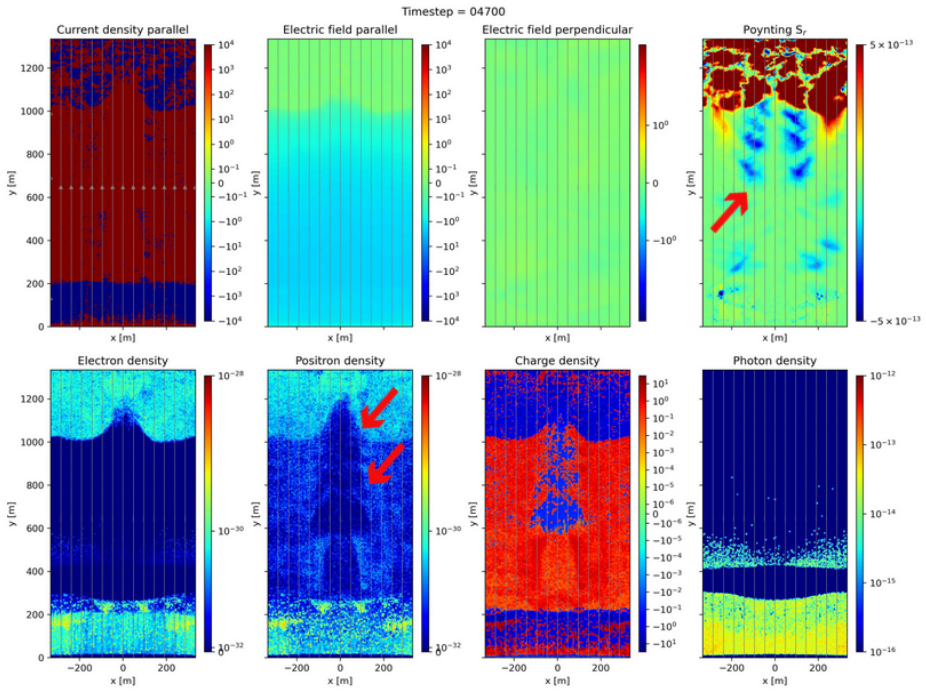

Figure 6.8: Reference simulation in a timestep 4700.

6.2.1 Time evolution of numbers of electrons, positrons and photons

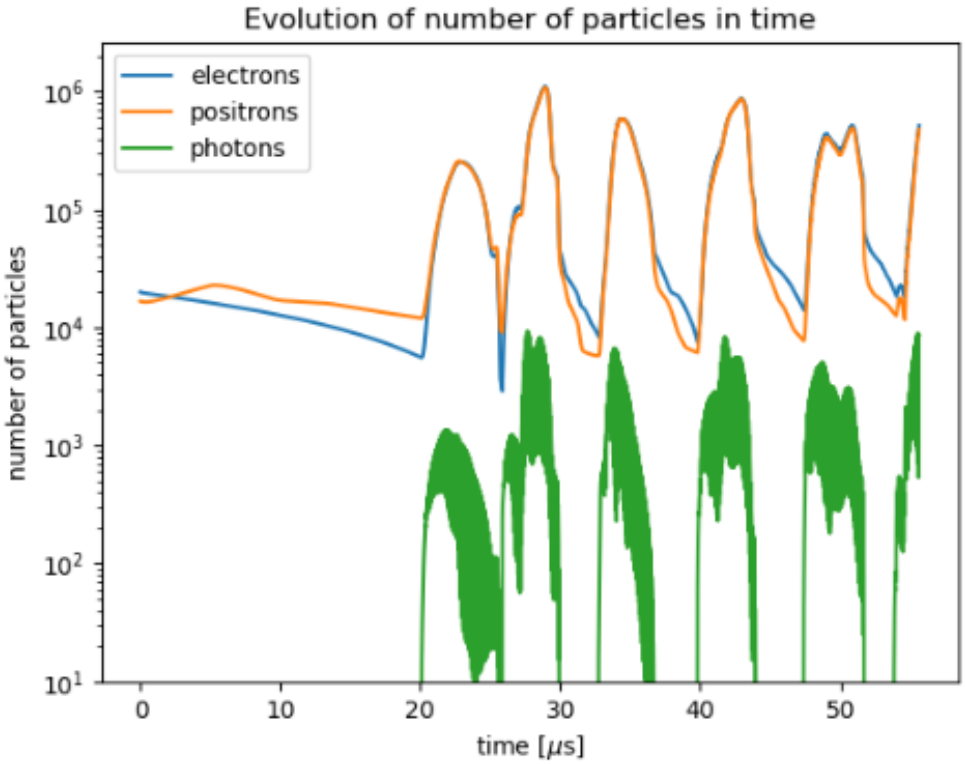

Figure 6.9: Time evolution of number of electrons, photons and positrons in the simulation domain.

In the Figure 6.9 we can see the time evolution of the number of electrons, positrons and photons. From the beginning, the number of electrons and positrons is slightly lowering, then starts the creation of photons at a time of 20 μs, and then beginning of the pair cascade occurs at time $20 - 21$ μs.

After some time we can see in the Figure 6.9 peaks in the number of particles – the evolution of quasi-periodic particle's cascades. Period of the process is $T_{ep} = 1175 \pm 34\Delta t = 6.5 \pm 0.2$ μs. That well corresponds to what we already know observationally (Beskin, Gurevich, and Istomin 1993), and therefore it seems that the code works as it should.

What is also important here are the photon quasi-periodic cascades. We can see that the growth of electrons corresponds to the growth of photons, exactly as it should. It is also interesting that all the photons leave the simulation before they are created again.

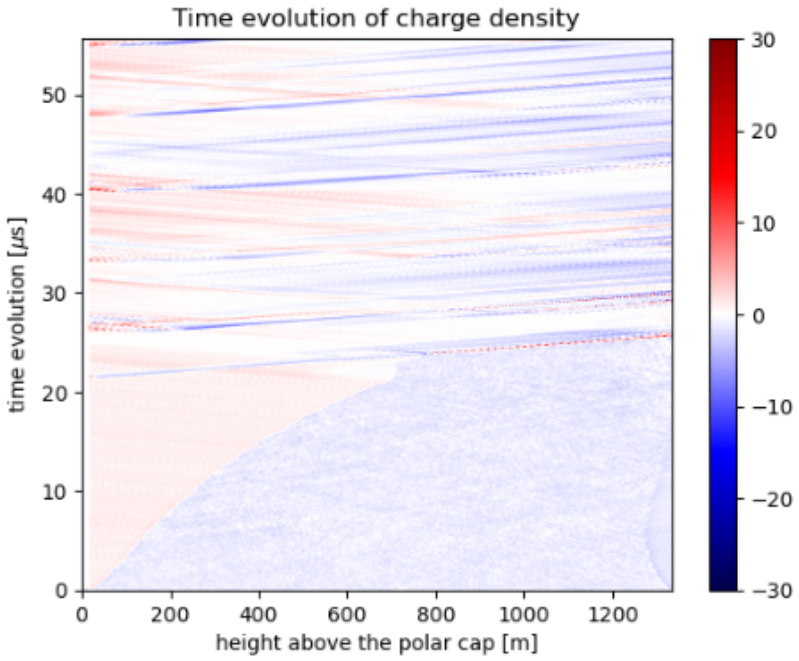

Figure 6.10: Time evolution of charge density in the center of simulation scaled to mean particle's density in the simulation.

Let us look closer at the time evolution of the density of the charged particles in the central grids of the simulation. In the Figure 6.10 we can see on the x-axis the height above the surface of the neutron star in the central grid of the simulation area. On the y-axis is the time evolution.

With the red color, there are illustrated areas with positive charge density and therefore with a higher number of positrons. Blue color represents the areas where more electrons occur than positrons. We can notice that at the beginning there are more electrons in the simulation domain. These electrons then start to outflow from the simulation and we see the growing positive charge density in the first 20 μs. This corresponds for example to what we see in the Figure 6.6. The charge density is scaled according to Equation (6.7).

6.2.2 Time evolution of electric and magnetic fields

In the Figure 6.11 we see the time evolution of energies of electric and magnetic fields, the energy of the external magnetic field is not included here. Electric field is scaled as in Equations (6.2) and (6.3).

The electric field grows at the beginning, with the motion of charged particles and then drops always when photons are created from the charged particle's interaction with the magnetic field, and again grows when new pairs are created.

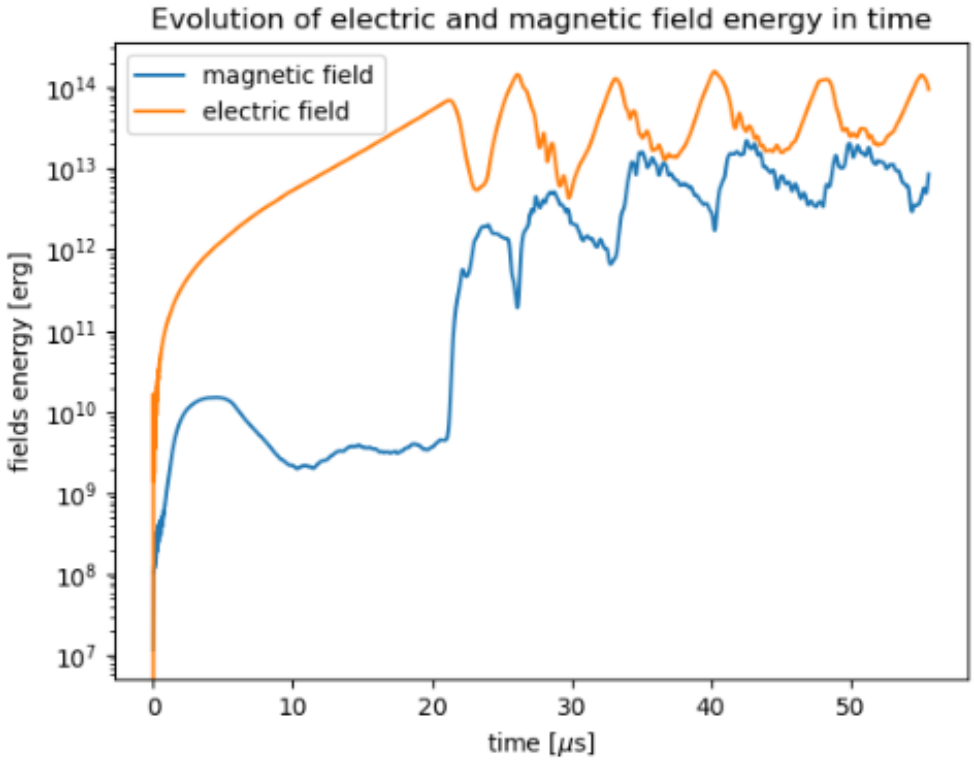

Figure 6.11: Time evolution of the energy of electric and magnetic field energy in the simulation domain.

What is interesting is that when the energy of the magnetic field grows, the energy of the electric field decreases. That could be the consequence of what we discuss in *Chapter 3.3*. The increasing number of particles starts to shield the electric field, therefore, it decreases, but those particles interact with the magnetic field, which then increases.

Now we can look at the time evolution of parallel electric field in the cross section of the simulation (Figure 6.12). What is important here is the white part of the image, where the parallel electric field is shielded and allows the outflow of the particles from the polar cap.

On the last Figure 6.13 is the time evolution of the perpendicular electric field in the central part of the simulation. We can see there that something starts to change after 20 μs, which corresponds to the creation of the first pair cascade. The red lines there could illustrate the motion of positively charged particles in the electric field in the direction towards the star. The blue lines then would correspond to the motion of negatively charged particles away from the star.

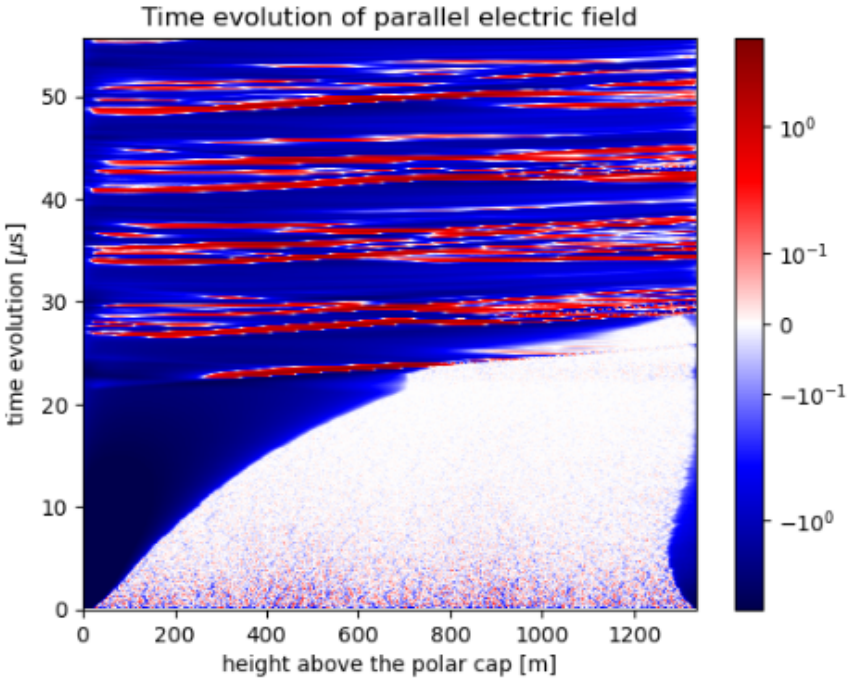

Figure 6.12: Time evolution of parallel electric field in the cut of the polar cap.

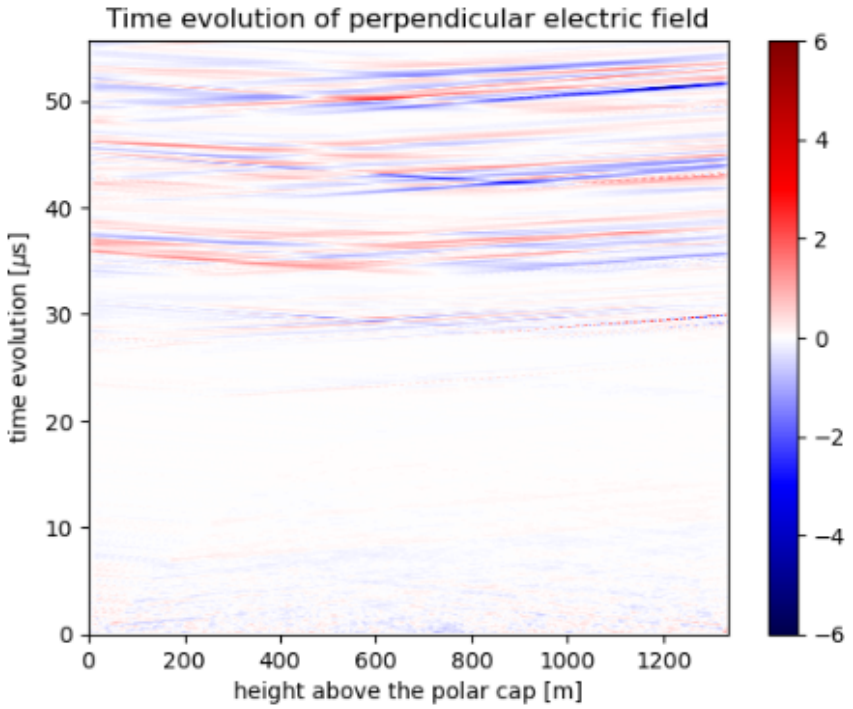

Figure 6.13: Time evolution of perpendicular electric field in the cut of the polar cap.

6.2.3 Dependence on the max_ppc

The parameter defining the maximal number of particles per cell seemed to have during tests an important role in the simulation.

On the Figure 6.14 below, we can see the impact on the number of electrons in the simulation. The first three cascades correspond to each other in the shape of the peeks and also in the period. The only difference is that the number of electrons is a higher for the simulations with higher allowed number of particles in a cell, which is natural. Also, we see that the difference between `max_ppc`= 100 and `max_ppc`= 1000 is not so noticeable, so maybe that would be an optimal number of particles in a cell.

Around 50 μs we see that cascades stop being regular and that the simulations with the higher number of particles in a cell evolve faster. That is possible, because the higher number of the particle in a cell can accelerate the process. In the Figure 6.15 of the time evolution of photons we can see the similar trend described as for the number of electrons.

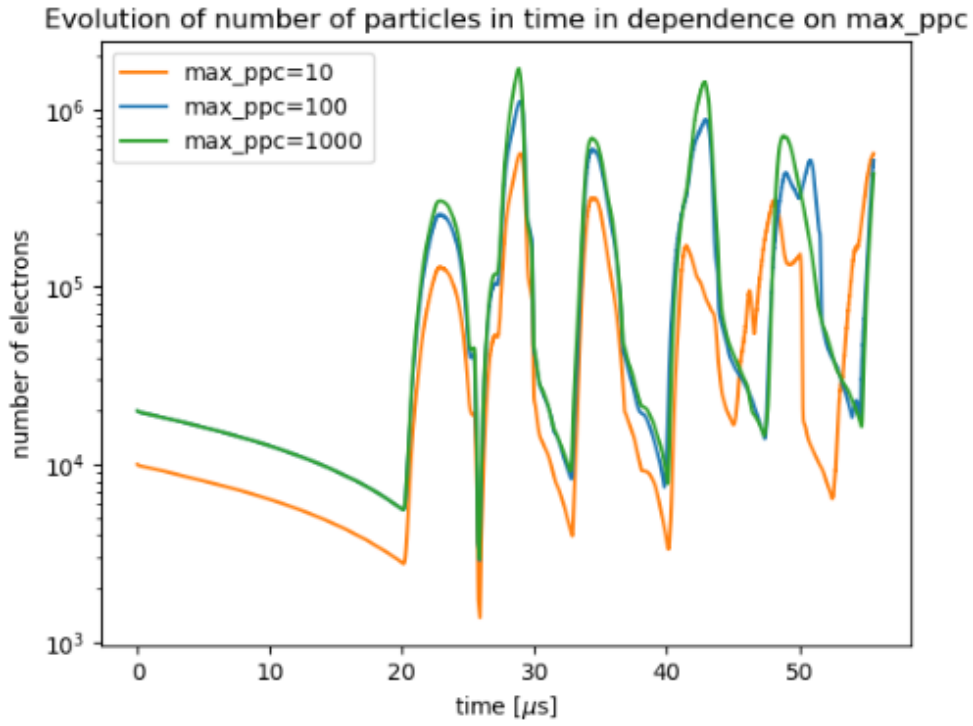

Figure 6.14: Time evolution of the number of electrons in the simulation domain in the dependence on `max_ppc`.

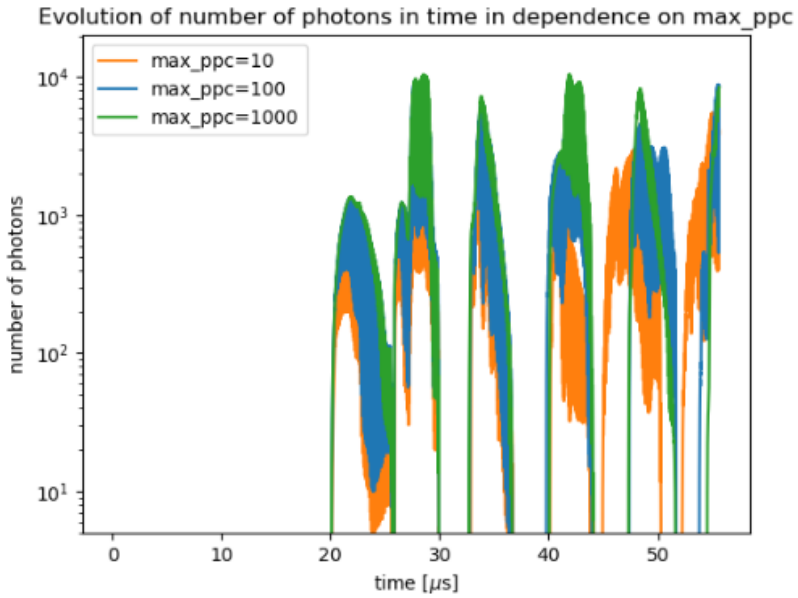

Figure 6.15: Time evolution of the number of photons in the simulation domain in the dependence on `max_ppc`.

6.2.4 Dependence on the photon_emission_threshold

This parameter have a large impact on the simulations. It showed that the simulations start to be numerically unstable after six thousand timesteps, and they are ending with a crash of the process.

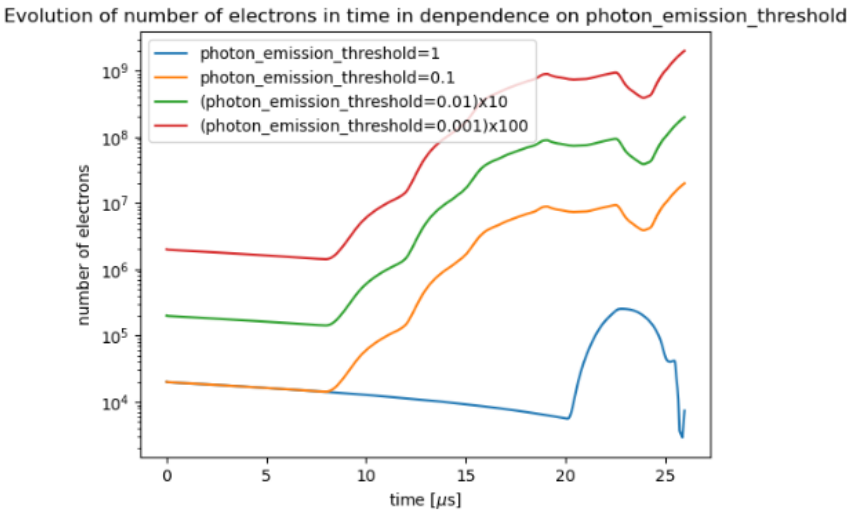

Figure 6.16: Time evolution of the number of electrons in the simulation domain in the dependence on `radiation_reaction_photon_emission_threshold`.

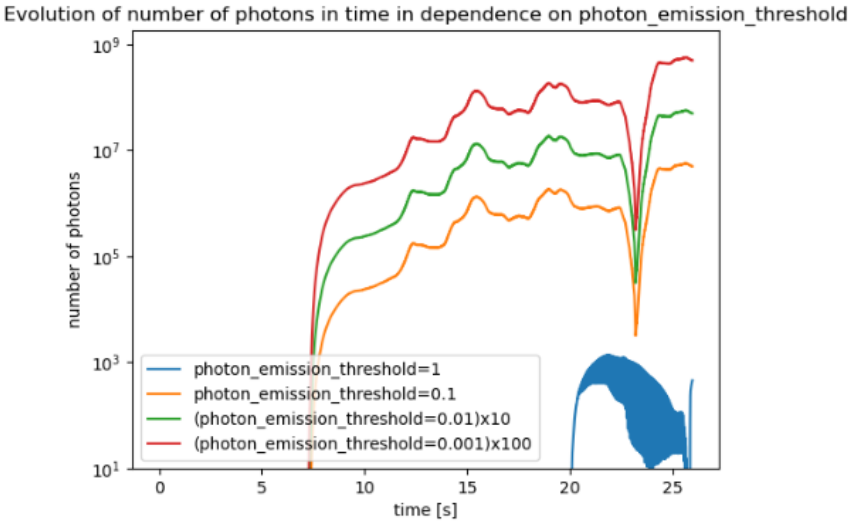

Figure 6.17: Time evolution of the number of photons in the simulation domain in the dependence on `radiation_reaction_photon_emission_threshold`.

As we see at the Figure 6.16 for the `photon_emission_threshold` with values 0.1, 0.01 and 0.001 is the shape of the function the same – for a better illustration the green function is the tenfold of the orange function, and red function is its hundredfold. The same procedure was applied also for the photon dependence.

What is interesting in both Figures 6.16 and 6.17 is that the progress of the simulation has the same shape for all values we have tried. From it we can say that an optimal value is either equal to 1, as in the reference simulation, or that it, at least, lies between 1 and 0.1.

6.2.5 Dependence on the curvature_radius

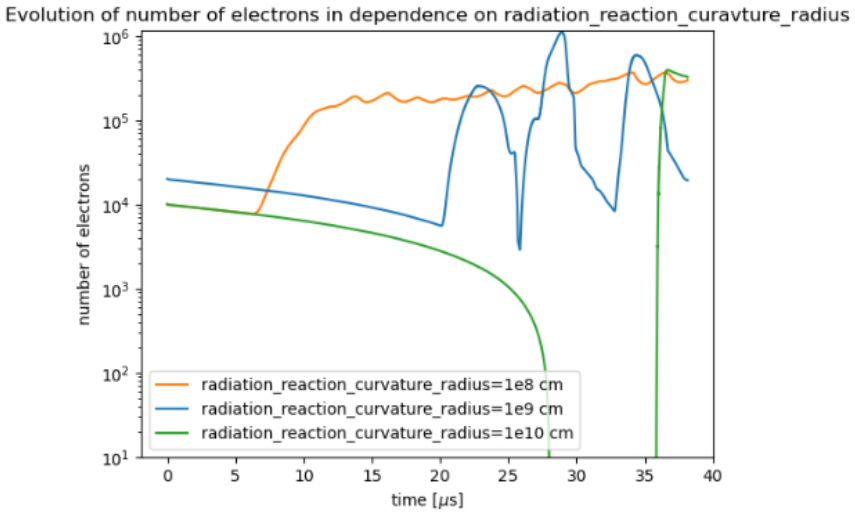

Figure 6.18: Time evolution of the number of electrons in the simulation domain in the dependence on `radiation_reaction_curvature_radius`.

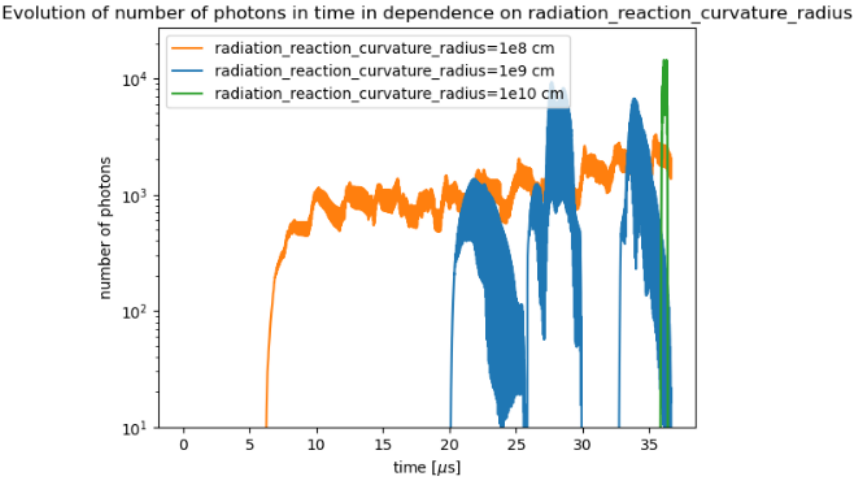

Figure 6.19: Time evolution of the number of photons in the simulation domain in the dependence on `radiation_reaction_curvature_radius`.

Next parameter we were examinig was `radiation_reaction_curvature_radius` which defines the radius of curvature of the magnetic field lines of the neutron star. As we see from the Figures 6.18 and 6.19, the biggest change is the time of generating the first cascade.

For our reference simulation with the curvature radius equal to 10^9 cm comes the first cascade around the 20 μs. For the simulation with higher curvature radius, it comes already around 6 μs and evolves faster and oscillates more. This is connected to the Equation (5.11), which tells us that the photons need to travel a shorter path, before they starts to create pairs. For the higher curvature radius simulation collapsed after the 6500 timesteps and ended after its first cascade at the time of 36 μs.

6.2.6 Dependence on the ν_{min} and ν_{max}

The last parameter we have tested was the range of ν_{min} and ν_{max}, given by parameters `radiation_reaction_nu_min` and `radiation_reaction_nu_max`, which are important when we are randomizing the selection of photon frequency from the function Equation (5.4). The simulation setup is in table below.

The parameters of simulation from *.cat* file	
max_ppc	100
`radiation_reaction_curvature_radius`	10^9 cm
`radiation_reaction_photon_emission_threshold`	1
`radiation_reaction_nu_min`	$0.01 \cdot \nu_{critical}$
`radiation_reaction_nu_max`	$10 \cdot \nu_{critical}$

Table 6.3: List of parameters used in the discussed simulation.

At the Figure 6.20 we can see that now the photon cascades are more regular and

at the same time there are more of them. Also the process stars sooner – around 10 μs.

To understand why, we need to define, how ν_{min} and ν_{max} influence the frequency of created photon ν_{photon}

$$\nu_{photon} = \nu_{min} + (\nu_{max} - \nu_{min}) \cdot r, \tag{6.9}$$

where r is the random number. For our reference simulation photon frequency was always equal to r. Now, when ν_{max} is ten times larger, the photon frequency can also be higher – and that can be the reason why the whole process is faster.

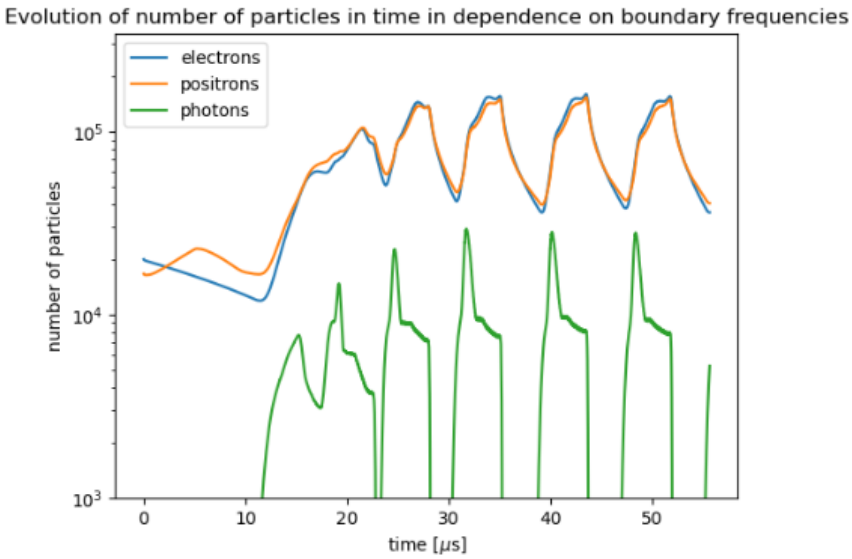

Figure 6.20: Time evolution of the number of photons in the simulation domain in the dependence on `radiation_reaction_nu_min` and `radiation_reaction_nu_max`.

Conclusion

In this thesis we were focusing on the investigation of plasma properties in the neutron star's magnetospheres. The main area of our interest was electron–positron plasma creation in the pulsar's polar caps.

For the examination of pulsar's magnetospheres we used the particle–in–cell code ACRONYM. We were working with its 2D version and we simulated the plasma pair creation in the area of the star's polar cap.

The main aim of this work was to implement into the code a new quantum electrodynamic condition for the creation of photons and electron–positron pairs in the simulation. This new condition takes into account the dependency of critical photon frequency on the particle's gamma factor and on the radius of curvature. Photons are selected randomly from the values given by the integral from the approximated Bessel function and are added into simulation according to comparison with the `radiation_reaction_photon_emission_threshold`. Particle pairs are created using the attenuation parameter α, from which is counted the conversion rate m that is also compared with a random number. This brings to an ACRONYM code a more complex view on a problem of electron–positron plasma creation, which is more accurate to the quantum electrodynamic approach.

After implementing this condition, we tested and debugged the code and we eliminated problems such as the particle sorting bug and others, then we started the testing of the code's numerical parameters. We were focusing especially on the parameters giving the maximal number of macroparticles per cell, photon emission threshold, radiation curvature radius and the boundary frequencies ν_{min} and ν_{max}.

We found out that the optimal maximal number of macroparticles per cell is 1000. We also found out that the optimal photon emission threshold is equal to 1 and that for the lower values, is the simulation unstable. We also found out that the best option for curvature radius is 10^8 cm. We also briefly tested the influence of the ν_{min} and ν_{max} and found out that with the involvement of this condition, simulation runs faster and more regular.

Finally, in all simulations we see working photon and electron–positron cascades, with period 6.5 ± 0.2 μs (for the reference simulation). From our results, we can say that the implementation of quantum electrodynamics into the code was successful, and we found how the numerical parameters are influencing its characteristics.

Bibliography

Benáček, Jan, Patricio A Muñoz, and Jörg Büchner (2021). "Bunch expansion as a cause for pulsar radio emissions". In: *The Astrophysical Journal* 923.1, p. 99.

Benáček, Jan, Andrey Timokhin, et al. (2024). "Poynting flux transport channels formed in polar cap regions of neutron star magnetospheres". In: *Astronomy & Astrophysics* 691, A137.

Beskin, Vasilij Semenovič, Aleksandr Viktorovich Gurevich, and Ya N Istomin (1993). *Physics of the pulsar magnetosphere*. Cambridge university press.

Bittencourt, José A (2013). *Fundamentals of plasma physics*. Springer Science & Business Media.

Bonaventura, Zdeněk (2026). "Introducion to Plasma Physics".

Erber, Thomas (Oct. 1966). "High-Energy Electromagnetic Conversion Processes in Intense Magnetic Fields". In: *Rev. Mod. Phys.* 38 (4), pp. 626–659. DOI: 10.1103/RevModPhys.38.626. URL: https://link.aps.org/doi/10.1103/RevModPhys.38.626.

Gotthelf, E. et al. (Aug. 2013). "X-RAY OBSERVATIONS OF DISRUPTED RECYCLED PULSARS: NO REFUGE FOR ORPHANED CENTRAL COMPACT OBJECTS". In: *The Astrophysical Journal* 773, p. 141. DOI: 10.1088/0004-637X/773/2/141.

Lorimer, Duncan Ross and Michael Kramer (2005). *Handbook of pulsar astronomy*. Vol. 4. Cambridge university press.

Nishikawa, Kenichi et al. (2021). "PIC methods in astrophysics: simulations of relativistic jets and kinetic physics in astrophysical systems". In: *Living Reviews in Computational Astrophysics* 7.1, p. 1.

Vay, J-L (2008). "Simulation of beams or plasmas crossing at relativistic velocity". In: *Physics of Plasmas* 15.5.

Appendix

Below we can see the *.cat* file of the reference simulation discussed in *Chapter 6*.

```
//Restart parameters
//restart_at=4000
//quit_after=3600
//gesamt_zeitschritte=2500

//Global domain size
nx0=200
nx1=400
nx2=1

//MPI domain decomposition
space_part_x=0
space_part_y=0
space_part_z=0

//MPI output tuning.Number of cpus writing to disk along
directions x/y
num_io_ranks_x=0
num_io_ranks_y=0

//Boundary conditions
bordertype_x=0
bordertype_y=2
bordertype_z=0

//Grid size and time step
rescale_dx=1.581
rescale_dt=0.98974404

//Particles per cell
electronnumberbg=1
positronnumberbg=1
electronnumberj=0
```

```
positronnumberj=0

//Physical parameters
mpzume=1
Bx=0.000000
By=0.01
Bz=0.0

//Physical scale
plasmafreq=4e6

//Temperature background
widthbg=0.1
widthj=0.1

//Relative drift speeds
vbgx=0.0
vbgy=0.0
vbgz=0.0
vjetx=0.0
vjety=0.0
vjetz=0.0
Bx0=0.0
By0=0.0
Bz0=0.0

gauss_cleaning=1
compensate_current=0
friedman_theta=0.1

//Default output frequency parameters
gesamt_zeitschritte=10000
output_zeitschritte=10
part_output_zeitschritte=1000
energy_output_zeitschritte=1
split_hdf_pertime=0
move_border_zeitschritte=0

//Lineout2 parameters.  Position=precise number of the grid
lineout2_zeitschritte=0
lineout2_position1_in_dim=1
lineout2_position1=0
lineout2_position2_in_dim=1
lineout2_position2=399
```

```
//Momenta parameters
momenta_output_zeitschritte=10
deposit_momenta_of=electron_bg, positron_bg, photon_bg
momenta_max_order=1.0

star_radius=1e6
star_mass=1e31
star_period=0.25
star_position_x=0
star_position_y=-1.065e6
star_polar_angle=0
star_azimuthal_angle=0
gravitation_force=0
fictitious_force=0
magnetospheric_current=1
magnetospheric_current_scale=5e-7
remove_at_star=1
reflect_at_star=0
generate_dipole=1
dipole_field=1e12
dipole_polar_angle=0.0
qed_gamma_threshold=100
qed_gamma_chi=0.1

boundary_inject_ppc_x=2
boundary_inject_ppc_y=2
boundary_star_surface_ppc=2
polar_cap_ppc=2
polar_cap_angle=2.5
polar_cap_dangle=0.01
fill_closed_lines_ppc=1
fill_closed_lines_macro_scale=1
fill_all_lines_ppc=1
absorb_waves_at_margins=0
absorb_waves_in_closed_fields=0
radiation_reaction_scale=1
radiation_reaction_curvature_radius=1e9
photon_maximal_distance=134217.6
radiation_reaction_gamma_min=1e7
max_ppc=100
radiation_reaction_curvature_losses=1
radiation_reaction_photon_emission_threshold=1
radiation_reaction_nu_max=1
radiation_reaction_nu_min=1
```